Engineering Structures 174 (2018) 322–337

Contents lists available at ScienceDirect

Engineering Structures

journal homepage: www.elsevier.com/locate/engstruct

Higher mode seismic structure-soil-structure interaction between adjacent building during earthquakes

Felipe Vicencio[a,*], Nicholas A. Alexander[b]

[a] Department of Civil Engineering, University of Bristol, Queen's Building, Bristol, UK
[b] Senior Lecturer in Structural Engineering, Department of Civil Engineering, University of Bristol, Queen's Building, Bristol, UK

ARTICLE INFO

Keywords:
Structure-Soil-Structure interaction (SSSI)
Time history seismic analysis
Dynamics

ABSTRACT

This paper evaluates the effect of Structure-Soil-Structure Interaction (SSSI) between two buildings under seismic excitation given different parameters of the buildings, inter-building spacing, and soil type. An extended simplified reduced-order model, that enables higher mode interaction between structures, is proposed. This enables the exploration of the interaction between buildings with a very large difference in height. A database of strong ground motions records with Far-Field, Near-Field Without Pulse and Near-Field Pulse-Like characteristics are employed. Over 3 million system/ground motion cases are analysed in this extensive parametric study. The results suggest that the extended model captures significant interactions, in displacement responses, for the cases of a small building closely flanked by a much taller one.

1. Introduction

During an earthquake, civil structures interact with the surrounding soil beneath their foundations. These structures are typically analysed (dynamically) as singleton structures, i.e. without any consideration of their neighbouring structures. This phenomenon is widely known as Soil-Structure Interaction (SSI), and the importance of including its beneficial or adverse structural effects has been the focus of attention for more than 40 years. Nevertheless, the existence of a high density of buildings in large cities inevitably results in the possibility of seismic interaction of adjacent buildings through the underlying soil. This problem is better known as Structure-Soil-Structure Interaction (SSSI) and has received more attention in recent years. The pioneering works of Luco and Contesse [1], Kobori et al. [2], Lee and Wesley [3], Murakami and Luco [4], Wong and Trifunac [5], Lysmer et al. [6], and Roesset and Gonzales [7] have emphasized the complexity of the problem and have investigated the importance of considering the dynamic coupling between several structures. Some early experimental studies at real or small scaled conducted by Mattiesen and MacCalden [8], and Koroby et al. [9] have also captured the SSSI effects.

More recent investigations have been developed based on numerical two or three-dimensional Finite Element Method (FEM), Boundary Elements Method (BEM) or a combination of these two FEM/BEM procedures. For example, the works of Qian and Beskos [10], Betti [11], Karabalis and Huang [12], Karabalis and Mohammadi [13], Lehmann and Antes [14], Qian et al. [15], Bard et al. [16], Yahyai et al. [17], Padron et al. [18], Bolisetti and Whittaker [19], among others. These studies have identified key factors that control the seismic interaction behaviour such as: (i) the inter-building distance, (ii) the direction of the alignment between foundations, (iii) the relative height and dynamic characteristics of adjacent buildings, (iv) the aspect ratio (the building height to width ratio), and (v) the soil class.

Discrete soil/foundation-spring models have been successfully applied in the evaluation of SSSI problems, where Mulliken and Karabalis [20,21] calculated the interaction between adjacent two and three identical rigid surface foundations supported by a homogeneous half-space soil, and subjected to impulsive, moment, sinusoidal and random loads. Recently, Alexander et al. [22] proposed a set of rotational springs to model the interaction between adjacent closely spaced buildings. These models were validated using finite element analyses. Aldaikh et al. [23,28] and Knappett et al. [29] extended the validation of these proposed interaction-spring models with both physical shake table and centrifuge tests. Additionally, Aldaikh et al. [24] proposed an alternative closed-form analytical expression for these interaction springs based on a Boussinesq approximation of the surficial displacement fields. These alternative formulae where shown to be completely consistent with those initially proposed and validated in [22,23,28]. Vicencio and Alexander [25] extended these previous models further by permitting the soil to exhibit nonlinear hysteretic behaviour. Results indicate that SSSI effects can increase with soil nonlinearity.

* Corresponding author.
E-mail address: fv16607@bristol.ac.uk (F. Vicencio).

https://doi.org/10.1016/j.engstruct.2018.07.049
Received 11 September 2017; Received in revised form 23 May 2018; Accepted 16 July 2018

Nomenclature

α_1, α_2	ratio of foundation/soil to building masses of buildings 1 and 2 respectively []
β	ratio of soil/foundation radii of gyration for buildings 1 and 2 []
ε	height ratio of buildings 2 to 1 []
η_1, η_2	height to radius of gyration ratios for buildings 1 and 2 respectively []
θ_1, θ_2	rotation at base of buildings 1 and 2 respectively []
κ	interaction spring between buildings 1 and 2 [$\mathrm{ML^2\,T^{-2}}$]
λ	ratio of mass polar moments of inertia of soil-foundation of buildings 2 to 1 []
μ	Poison's ratio of soil []
ξ_n	critical damping of the system []
ρ_b, ρ_s	average densities of building and soil respectively [$\mathrm{M\,L^{-3}}$]
τ	scaled time []
ϕ_n	modal eigenvector of the system []
χ_{ii}	percentage change in total displacement power when moving from uncoupled to coupled state [%]
$\ddot{\chi}_{ii}$	percentage change in total acceleration power, moving from uncoupled to coupled state [%]
ω_{rb1}	modal circular frequency on rock of building 1 [$\mathrm{rad\,T^{-1}}$]
ω_{b1}	frequency parameter of building 1 [$\mathrm{rad\,T^{-1}}$]
ω_{b2}	frequency parameter of building 2 [$\mathrm{rad\,T^{-1}}$]
ω_{s1}	freq. parameter of soil/foundation building 1 [$\mathrm{rad\,T^{-1}}$]
ω_{s2}	freq. parameter of soil/foundation building 2 [$\mathrm{rad\,T^{-1}}$]
ω	Fourier frequency [$\mathrm{rad\,T^{-1}}$]
ω_n	natural frequencies of the systems [$\mathrm{rad\,T^{-1}}$]
ϖ	interaction frequency ratio parameter [$\mathrm{rad\,T^{-1}}$]
Ω_0	ratio of interaction to building 1 frequency parameter []
Ω_2	ratio of building 1 (soil/foundation) to building 1 frequency parameter []
Ω_3	ratio of building 2 to building 1 circular frequencies []
Ω_4	ratio of building 2 (soil/foundation) to building 1 circular frequencies []
A_1, A_2	total non-dimensional acceleration of building 1 []
A_3, A_4	total non-dimensional acceleration of building 2 []
b	foundation width []
$\mathbf{C}$	non-dimensional damping matrix []
$\widehat{\mathbf{C}}$	dimensional damping matrix [$\mathrm{MT^{-1}}$]
c_1	density ratio (soil/buildings) parametric constant []
c_2	frequency ratio parametric constant []
E_s	total power spectral density []
h_1, h_2	total heights of building 1 and 2 respectively [L]
$\mathbf{K}$	non-dimensional stiffness matrix []
$\widehat{\mathbf{K}}$	dimensional stiffness matrix [$\mathrm{MT^{-2}}$]
k_s	soil/foundation rotational spring in absence of building interaction [$\mathrm{ML^2\,T^{-2}}$]
k_{b1}, k_{b2}	lateral stiffnesses of building 1 and 2 resp. [$\mathrm{MT^{-2}}$]
k_{s1}, k_{s2}	rotational soil stiffnesses of soil beneath building 1 and 2 respectively [$\mathrm{ML^2\,T^{-2}}$]
$\mathbf{M}$	non-dimensional mass matrix []
$\widehat{\mathbf{M}}$	dimensional mass matrix [M]
M_w	moment magnitude scale
m_{b1}, m_{b2}	total masses of building 1 and 2 respectively [M]
m_{s1}, m_{s2}	soil/foundation masses underneath building 1 and 2 respectively [M]
	non-dimensional force vector []
$\widehat{\mathbf{p}}$	dimensional force vector [$\mathrm{ML\,T^{-2}}$]
r_1, r_2	soil/foundation masses radius of gyration of building 1 and 2 respectively [L]
s	aspect ratio of building 1 []
T_E	system kinematic energy [$\mathrm{ML^2T^{-2}}$]
t	time [T]
U_1, U_2	total non-dimensional relative displacement to ground of building 1 []
U_3, U_4	total non-dimensional relative displacement to ground of building 2 []
U_E	system potential energy [$\mathrm{ML^2\,T^{-2}}$]
$U_i(\omega)$	Fourier transform of $U_i(\tau)$
u_1, u_2	non-dimensional relative displacement to ground of building 1 []
u_3, u_4	non-dimensional relative displacement to ground of building 2 []
u_g	non-dimensional horizontal ground displacement time series []
$\ddot{u}_g$	non-dimensional acceleration ground motion []
$\mathbf{u}$	non-dimensional degree of freedoms vector []
V_s	shear wave velocity of soil [$\mathrm{L\,T^{-1}}$]
$\overline{V}_s$	normalised non-dimensional shear wave velocity of soil []
$\mathbf{v}_{b1}(\omega)$	displacement transfer function for building 1
$\mathbf{v}_{b2}(\omega)$	displacement transfer function for building 2
$\ddot{\mathbf{v}}_{b1}(\omega)$	acceleration transfer function for building 1
$\ddot{\mathbf{v}}_{b2}(\omega)$	acceleration transfer function for building 2
x_1, x_2	relative displacement to ground (in a rotating coordi-nate frame) of building 1 [L]
x_3, x_4	relative displacement to ground (in a rotating coordi-nate frame) of building 2 [L]
x_g	horizontal ground displacement time series [L]
$\ddot{x}_g$	horizontal acceleration ground motion [$\mathrm{L\,T^{-2}}$]
$\mathbf{x}$	dimensional degree of freedoms vector []
z	non-dimensional inter-building distance []

Hans et al. [26] and Li et al. [27] have conducted some experimental in situ investigation, at real or small scales, which used a series of shaking table test to study the effects of SSSI on the response of buildings. Trombetta et al. [30,31] and Mason et al. [32] have investigated the SSSI effects using physical models in centrifuge tests. Kitada et al. [33] and Yano et al. [34] studied the SSSI problem for nuclear plants in the field and developed laboratory tests.

Experimental tests of specific cases are essential as validation points. However, we should be under no illusions; these experiments are challenging to undertake. This is because of the problems of scaling. Results represent a statistically small sample, and inevitably they provide only a limited parametric exploration of the generalised problem. Some would advocate that advanced computational models (FEA) that are the obvious choice for exploring these problems. However, it is very difficult to characterise both structures and soil in a general and generic sense for a whole class of building configurations. Thus, large-scale parametric exploration of this problem is difficult to achieve with these approaches. In some sense, the burden of information required (in terms of ground motion, building geometry and material parameters) for the specification of advanced computational models can obscure insights into the problem as there are too many system parameters to explore. Therefore, an alternative approach are parametric studies using reduced order models with a relatively limited number of degrees of freedom. These reduced-order models (i) capture the most significant dynamic behaviour (ii) have a relatively small number of system parameters and (iii) are computationally simple enough for exploring a huge number of generic cases. These parametric studies should be viewed as an initial exploration of the problem. They are not meant to replace advanced computational models and experimental work of specific cases.

In this paper, over 3.1 million of different time-histories cases are explored using the BlueCrystal, the High-Performance Computing (HPC) machine belonging to the Advance computing research centre at the University of Bristol.

1.1. Aims

In this study, we extend the previous work on the SSSI of two buildings [22], by including an additional degree of freedom (DOF) for each of the buildings. Note that the interaction-springs in [22] were validated with finite element analyses [23], shake table tests [28], centrifuge test [29] and matched closed-form analytical expressions [24]. This extra building DOF enables an extra mode for each structure. Hence, we can extend the parametric scope of the previous study to include the case of a low-rise building adjacent to a neighbouring much taller building. Additionally, we shall now employ real ground motion rather than a Kanai-Tajimi artificial ground motion. These are classified into three groups: Far-Field (FF), Near-Field Without Pulse (NFWP) and Near-Field Pulse-Like (NFPL) [35]. These ground motions have differences in amplitude, duration, envelope shape, and power spectral content. The previous paper highlighted the possibility that the power of the earthquake passed from the taller structure to the smaller structure when the height ratio is close to 1.1 (i.e. the second building is 10% taller than the first building), and the buildings are closely spaced. The aim of this paper is to answer the following questions.

- Does the introduction of additional degrees of freedom (and hence modes) in the buildings influence the size of adverse/beneficial SSSI behaviour?
- Is there evidence to suggest that different types of ground motion (FF, NFWP and NFPL) can affect the SSSI behaviour?
- Do displacement responses follow a similar trend to total acceleration responses?

2. A theoretical reduced order model for SSSI

2.1. Non-dimensional equations of motion

A two buildings system is shown in Fig. 1, and is described in terms of six degrees of freedom (DOF). Buildings are coupled with a rotational interaction spring κ. The soil/foundation system of each building has one rotational DOF at the foundation level θ_j. The building superstructures have two translational DOFs (x_{2j-1} and x_{2j}) relative to the ground, with $j \in [1, 2]$. Thus, the three DOFs of each building can be viewed as a projection, onto a three modes vector basis, of a generalised multi-storey building of height h_j. In the same way, this extended simplified reduced model enables SSSI between the 'second sway mode' of a tall building and the 'first sway mode' of a shorter building that was neglected in previous studies [22,23]. A known ground displacement field x_g is applied at both foundations, i.e. wave passage effects and spatially heterogeneous ground displacement are neglected in the present work. Building pounding is not permitted as inter-building spacing is assumed large enough to avoid pounding.

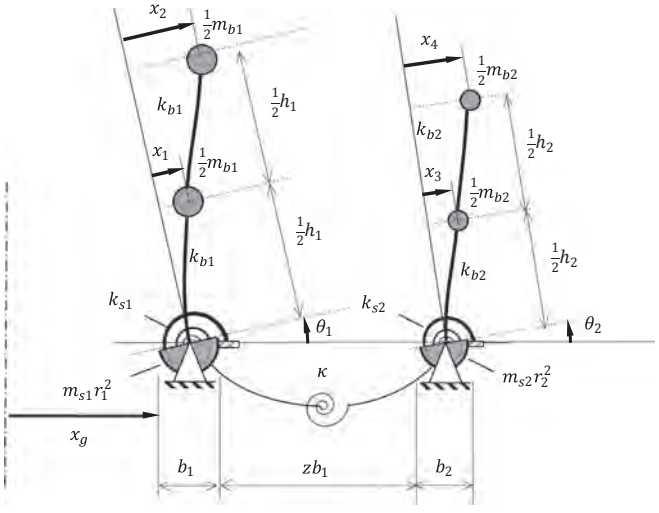

Fig. 1. Two building system.

The kinetic energy T_E and potential energy U_E for this system are given by Eqs. (1) and (2) respectively. The total kinetic energy can be specified as the sum of translational kinetic energy (due to sway and foundation rotation) of each building's mass and the rotational energies of each foundation/soil mass. The potential energy is the sum of internal work due to buildings deformation, rotation of the foundation springs underneath the buildings, and the differential rotation between buildings.

$$T_E = \frac{1}{2}\sum_{j=1}^{2}\left(\frac{1}{2}m_{bj}\left(\dot{x}_{2j-1} + \dot{x}_g - \frac{1}{2}h_j\dot{\theta}_j\right)^2 + \frac{1}{2}m_{bj}(\dot{x}_{2j} + \dot{x}_g - h_j\dot{\theta}_j)^2 + m_{sj}r_j^2\dot{\theta}_j^2\right) \tag{1}$$

$$U_E = \frac{1}{2}\sum_{j=1}^{2}\left(k_{bj}x_{2j-1}^2 + k_{bj}(x_{2j} - x_{2j-1})^2 + k_{sj}\theta_j^2\right) + \frac{1}{2}\kappa(\theta_2 - \theta_1)^2 \tag{2}$$

where h_j is the total height of the buildings and m_{bj} is the total mass of the buildings. m_{sj} are the foundation/soil masses underneath building 1 and 2, r_j are the soil/foundation masses radius of gyration, $m_{sj}r_j^2$ are the foundation/soil mass polar second moments of area (moments of inertia). k_{bj} are the building lateral stiffnesses, κ is the stiffness of the inter-building soil rotational spring and b_j are the width of the buildings' foundation. The Euler-Lagrange equation of motion describing the dynamics of the discretised system can be derived in the standard way by calculus and is formulated in Eq. (3).

$$\widehat{\mathbf{M}}\ddot{\mathbf{x}} + \widehat{\mathbf{C}}\dot{\mathbf{x}} + \widehat{\mathbf{K}}\mathbf{x} = \widehat{\mathbf{p}}\ddot{x}_g \tag{3}$$

where the system matrices are defined as follows,

$$\widehat{\mathbf{M}} = \begin{bmatrix} \frac{1}{2}m_{b1} & 0 & -\frac{1}{4}m_{b1}h_1 & 0 & 0 & 0 \\ 0 & \frac{1}{2}m_{b1} & -\frac{1}{2}m_{b1}h_1 & 0 & 0 & 0 \\ -\frac{1}{4}m_{b1}h_1 & -\frac{1}{2}m_{b1}h_1 & \frac{5}{8}m_{b1}h_1^2 + m_{s1}r_1^2 & 0 & 0 & 0 \\ 0 & 0 & 0 & \frac{1}{2}m_{b2} & 0 & -\frac{1}{4}m_{b2}h_2 \\ 0 & 0 & 0 & 0 & \frac{1}{2}m_{b2} & -\frac{1}{2}m_{b2}h_2 \\ 0 & 0 & 0 & -\frac{1}{4}m_{b2}h_2 & -\frac{1}{2}m_{b2}h_2 & \frac{5}{8}m_{b2}h_2^2 + m_{s2}r_2^2 \end{bmatrix} \tag{4}$$

$$\widehat{\mathbf{K}} = \begin{bmatrix} 2k_{b1} & -k_{b1} & 0 & 0 & 0 & 0 \\ -k_{b1} & k_{b1} & 0 & 0 & 0 & 0 \\ 0 & 0 & k_{s1} + \kappa & 0 & 0 & -\kappa \\ 0 & 0 & 0 & 2k_{b2} & -k_{b2} & 0 \\ 0 & 0 & 0 & -k_{b2} & k_{b2} & 0 \\ 0 & 0 & -\kappa & 0 & 0 & k_{s2} + \kappa \end{bmatrix}$$

$$\widehat{\mathbf{p}} = \begin{bmatrix} -\frac{1}{2}m_{b1} \\ -\frac{1}{2}m_{b1} \\ \frac{3}{4}m_{b1}h_1 \\ -\frac{1}{2}m_{b2} \\ -\frac{1}{2}m_{b2} \\ \frac{3}{4}m_{b2}h_2 \end{bmatrix}, \quad \mathbf{x} = \begin{bmatrix} x_1 \\ x_2 \\ \theta_1 \\ x_3 \\ x_4 \\ \theta_2 \end{bmatrix} \tag{5}$$

The dimensional form of the system (3) contains too many system parameters. This is a rather large number for a parametric study even in a linear system. Hence, we seek a reduction in the number of parameters through a process of removing all system dimensions. Thereby, we can

introduce the following non-dimensional parameter groups,

$$\eta_1 = \frac{h_1}{r_1},\ \eta_2 = \frac{h_2}{r_2},\ \alpha_1 = \frac{m_{s1}}{m_{b1}},\ \alpha_2 = \frac{m_{s2}}{m_{b2}},\ \beta = \frac{r_1}{r_2},\ \lambda = \frac{m_{b2}r_2^2}{m_{b1}r_1^2} \tag{6}$$

the frequency parameters,

$$\omega_{b1}^2 = \frac{k_{b1}}{m_{b1}},\ \omega_{s1}^2 = \frac{k_{s1}}{m_{s1}r_1^2},\ \omega_{b2}^2 = \frac{k_{b2}}{m_{b2}},\ \omega_{s2}^2 = \frac{k_{s2}}{m_{s2}r_2^2},\ \varpi^2 = \frac{\kappa}{m_{b1}r_1^2} \tag{7}$$

and the non-dimensional frequency ratios normalised by ω_{b1},

$$\Omega_2 = \frac{\omega_{s1}}{\omega_{b1}},\quad \Omega_3 = \frac{\omega_{b2}}{\omega_{b1}},\quad \Omega_4 = \frac{\omega_{s2}}{\omega_{b1}},\quad \Omega_0 = \frac{\varpi}{\omega_{b1}} \tag{8}$$

To define the properties of the system, we seek to estimate the system parameter ω_{b1}, which can be related to the first modal circular frequency (on a fixed base) ω_{rb1} for the building 1. If the equation of motion (3) is derived for a rigid base case, as shown in Appendix A, then static condensation of the above equation of motion (3) results in a two-DOF system. The first modal circular frequency ω_{rb1} of this system can be obtained by the solution of its resulting eigenvalue problem, as follow.

$$\omega_{rb1} = 0.874\sqrt{\frac{k_{b1}}{m_{b1}}} = 0.874\omega_{b1} \tag{9}$$

In this paper, we approximated the first building frequency ω_{rb1} by using the SEAOC Blue Book [36] estimate of the natural period of a structure on a rigid foundation, that is $T = n_S/10$ (where T is the fundamental natural period of a structure in seconds, and n_S is the number of storeys). If we assume an average storey height of 3.2 m, the total height of the building is $h_1 = 3.2n_s$ and hence the period is $T = h_1/32$. The period has a relationship with the circular frequency of $\omega_{rb1} = 2\pi/T$. Therefore, the fundamental natural frequencies, on a rigid base, are $\omega_{rb1} \approx 200/h_1$ and $\omega_{rb2} \approx 200/h_2$ for the building 1 and 2 respectively. Thus, we can re-express the frequency parameters described in Eq. (7) for the buildings 1 and 2 in terms of buildings' height.

$$\omega_{b1} \approx \frac{228.83}{h_1},\quad \omega_{b2} \approx \frac{228.83}{h_2} \tag{10}$$

Finally, we introduce the following change of variables $x_{2j-1} = u_{2j-1}r_j$, $x_{2j} = u_{2j}r_j$, $x_g = u_g r_1$ and the time scale $\tau = \omega_{b1}t$. This completes the full non-dimensionalisation of the problem, where u_{2j-1} and u_{2j} are the non-dimensional relative displacement of buildings to ground and u_g is the non-dimensional horizontal ground displacement (absolute). Therefore, after some calculus, the Euler-Lagrange equations of motion can be stated thus,

$$\mathbf{M\ddot{u}} + \mathbf{C\dot{u}} + \mathbf{Ku} = \mathbf{p}\ddot{u}_g \tag{11}$$

where Newtonian dots above now indicated derivatives with respect to scaled time τ, i.e. $(\dot{\bullet}) = \partial/\partial\tau$ and $(\ddot{\bullet}) = \partial^2\bullet/\partial\tau^2$. The matrices and vectors for the above equation are stated as follows,

$$\mathbf{M} = \frac{1}{2}\begin{bmatrix} 1 & 0 & -\frac{1}{2}\eta_1 & 0 & 0 & 0 \\ 0 & 1 & -\eta_1 & 0 & 0 & 0 \\ -\frac{1}{2}\eta_1 & -\eta_1 & \frac{5}{4}\eta_1^2 + 2\alpha_1 & 0 & 0 & 0 \\ 0 & 0 & 0 & \lambda & 0 & -\frac{1}{2}\eta_2\lambda \\ 0 & 0 & 0 & 0 & \lambda & -\eta_2\lambda \\ 0 & 0 & 0 & -\frac{1}{2}\eta_2\lambda & -\eta_2\lambda & \left(\frac{5}{4}\eta_2^2 + 2\alpha_2\right)\lambda \end{bmatrix} \tag{12}$$

$$\mathbf{K} = \begin{bmatrix} 2 & -1 & 0 & 0 & 0 & 0 \\ -1 & 1 & 0 & 0 & 0 & 0 \\ 0 & 0 & \alpha_1\Omega_2^2 + \Omega_0^2 & 0 & 0 & -\Omega_0^2 \\ 0 & 0 & 0 & 2\lambda\Omega_3^2 & -\lambda\Omega_3^2 & 0 \\ 0 & 0 & 0 & -\lambda\Omega_3^2 & \lambda\Omega_3^2 & 0 \\ 0 & 0 & -\Omega_0^2 & 0 & 0 & \alpha_2\lambda\Omega_4^2 + \Omega_0^2 \end{bmatrix}$$

$$\mathbf{p} = \frac{1}{2}\begin{bmatrix} -1 \\ -1 \\ \frac{3}{2}\eta_1 \\ -\lambda\beta \\ -\lambda\beta \\ \frac{3}{2}\eta_1\lambda\beta \end{bmatrix},\quad \mathbf{u} = \begin{bmatrix} u_1 \\ u_2 \\ \theta_1 \\ u_3 \\ u_4 \\ \theta_2 \end{bmatrix} \tag{13}$$

The system's linear viscous damping matrix $\mathbf{C}$ defined in equation (11) assumes that each natural mode $n \in [1, 6]$ is damped at $\xi_n = 0.05$ of critical damping. $\boldsymbol{\phi}_n$ is the eigenvector for mode n, ω_n are the natural frequencies of the systems. Thus, the Caughey orthogonal damping matrix $\mathbf{C}$ can be calculated as [37]:

$$\mathbf{C} = \mathbf{M}\left(\sum_{n=1}^{6} \frac{2\xi_n\omega_n}{\boldsymbol{\phi}_n^T\mathbf{M}\boldsymbol{\phi}_n}\boldsymbol{\phi}_n\boldsymbol{\phi}_n^T\right)\mathbf{M} \tag{14}$$

2.2. Reducing the number of system parameters

Eq. (11) is expressed in terms of ten linear system parameters η_1, η_2, α_1, α_2, λ, Ω_0, Ω_2, Ω_3, Ω_4 and ω_{b1}. Additionally, the ground excitation has its own statistical descriptors which can be viewed as further system parameters. Therefore, we still have a large system parameter space to explore for a comprehensive parametric study. To reduce this number, we follow the procedure described in [22] where the scope of our analysis is limited by assuming that:

(i) *the same soil profile exists under both buildings, this means* $k_{s1} = k_{s2}$
(ii) *both buildings have a similar square plan area of* b^2, *where* $r_1 = r_2 = 0.33b$
(iii) *both buildings have the same average density,* ρ_b
(iv) *the buildings can be of different heights,* h_j
(v) *the buildings are spaced at some arbitrary distance from each other,* zb.

Newmark and Rosenblueth [38] proposed that the dynamic mass of soil beneath buildings is equal to $m_s = 0.35b^3\rho_s$. The mass of the buildings can be calculated as $m_{bj} = \rho_b h_j b^2$, where ρ_s and ρ_b are the densities of soil and building respectively. Based on typical spans and floor loading, the average building density is 400–800 kg/m^3, while typical soil density ranges between 1200–2100 kg/m^3. Hence, the soil density and the proportionality constant c_1 used in this research is defined in Table 1. The radius of gyration of the soil-cylinder (directly under the rigid foundation) is calculated according to the Newmark's empirical expression $r \approx 0.33b$. Parameters η_1, η_2, α_1, α_2 and λ are contracted into two geometric parameters *Height ratio* $\varepsilon = \frac{h_2}{h_1}$ and *Aspect ratio* $s = \frac{h_1}{b}$.

$$\eta_1 = 3s,\ \eta_2 = 3\varepsilon s,\ \alpha_1 = \frac{c_1}{s},\ \alpha_2 = \frac{c_1}{\varepsilon s},\ \lambda = \varepsilon,\ c_1 = 0.35\frac{\rho_s}{\rho_b} \tag{15}$$

Empirical forms for the rotational and inter-building interaction spring defined in Alexander et al. [22] are used. These values were validated using finite element models, physical experimental models and closed-form analytical models [22–24,28]. Therefore, the values of foundation rotational spring $k_{s1} = k_{s2} = k_s q_2$, and the interaction spring stiffness κ is modelled as an inverse cube function of non-dimensional inter-building separation distance z.

Table 1
Linear elastic stiffness parameters for soil classes.

Soil class (sand)	$\rho_s[kg/m^3]$	$\mu[]$	$c_1[]$	$c_2[]$	$V_s[m/s]$
Dense	2000	0.35	1.17	385.4	325
Medium	1600	0.30	0.93	357.9	250
Loose	1300	0.30	0.76	357.9	156

$$\kappa = q_k q_2 k_s,\ q_k = -\frac{0.25}{(1+z)^3},\ q_2 = 1 + \frac{0.5}{(1+z)^3},\ k_s = \frac{1}{2}\frac{G_s b^3}{1-\mu} \tag{16}$$

The rotational stiffness spring coefficient k_s is obtained by using the empirical formula (deduced by Gorbunov-Possadov et al. [39]) in the absence of building interaction. G_s is the elastic shear modulus of the soil and μ is the Poisson's ratio of the soil. Hence, we can express the soil frequency ratios in the form,

$$\omega_{s1}^2 = \omega_{s2}^2 = \frac{k_{s1}}{m_{s1} r_1^2} = \frac{\frac{1}{2}\frac{G_s b^3}{1-\mu} q_2}{(0.35 b^3 \rho_s)(0.33b)^2} = 13.1 \times 10^6 \frac{1}{1-\mu}\frac{1}{b^2} q_2 \overline{V}_s^2 \tag{17}$$

$$\Omega_2^2 = \Omega_4^2 = \frac{\omega_{s1}^2}{\omega_{b1}^2} = \frac{13.1 \times 10^6 \frac{1}{1-\mu}\frac{1}{b^2} q_2 \overline{V}_s^2}{\frac{228.23^2}{h_1^2}} = c_2 q_2 \overline{V}_s^2 s^2,\ c_2 = \frac{250.52}{1-\mu} \tag{18}$$

where $V_s = \sqrt{G_s/\rho_s}$ is the shear wave velocity of the soil in [m/s], $\overline{V}_s = V_s/1000$ is the normalised non-dimensional shear wave velocity (to a reference of 1000 m/s) and soil constant c_2; both are defined in table 1. The frequency ratio parameters Ω_0 and Ω_3, the ratio of foundation radii of gyration β and the ratio of foundation mass polar moments of inertia $\lambda = \beta$ are contracted and re-expressed in terms of:

$$\Omega_0^2 = \frac{\kappa}{\omega_{b1}^2 m_{b1} r_1^2} = \frac{\frac{1}{2}\frac{G_s b^3}{1-\mu} q_2 q_k}{\frac{228.23^2}{h_1^2}(\rho_b h_1 b^2)(0.33b)^2} = c_1 c_2 q_2 q_k s \overline{V}_s^2,\ \Omega_3 = \frac{1}{\varepsilon} \tag{19}$$

Thus, Eqs. (12) and (13) can re-express as follows,

$$\mathbf{M} = \frac{1}{2}\begin{bmatrix} 1 & 0 & -\frac{3}{2}s & 0 & 0 & 0 \\ 0 & 1 & -3s & 0 & 0 & 0 \\ -\frac{3}{2}s & -3s & \frac{45}{4}s^2 + 2c_1 s^{-1} & 0 & 0 & 0 \\ 0 & 0 & 0 & \varepsilon & 0 & -\frac{3}{2}\varepsilon^2 s \\ 0 & 0 & 0 & 0 & \varepsilon & -3\varepsilon^2 s \\ 0 & 0 & 0 & -\frac{3}{2}\varepsilon^2 s & -3\varepsilon^2 s & \frac{45}{4}\varepsilon^3 s^2 + 2c_1 s^{-1} \end{bmatrix} \tag{20}$$

$$\mathbf{K} = \begin{bmatrix} 2 & -1 & 0 & 0 & 0 & 0 \\ -1 & 1 & 0 & 0 & 0 & 0 \\ 0 & 0 & c_1 c_2 q_2 s \overline{V}_s^2 (1+q_k) & 0 & 0 & -c_1 c_2 q_2 q_k s \overline{V}_s^2 \\ 0 & 0 & 0 & 2\varepsilon^{-1} & -\varepsilon^{-1} & 0 \\ 0 & 0 & 0 & -\varepsilon^{-1} & \varepsilon^{-1} & 0 \\ 0 & 0 & -c_1 c_2 q_2 q_k s \overline{V}_s^2 & 0 & 0 & c_1 c_2 q_2 s \overline{V}_s^2 (1+q_k) \end{bmatrix}$$

$$\mathbf{p} = \frac{1}{2}\begin{bmatrix} -1 \\ -1 \\ \frac{9}{2}s \\ -\varepsilon \\ -\varepsilon \\ \frac{9}{2}\varepsilon^2 s \end{bmatrix} \tag{21}$$

Therefore, in this analysis, we need only 3 geometric non-dimensional parameters and one site classification. This allows us to perform an intensive study that explores a huge number of generic cases. Hence, the complete problem, in Eq. (11), is reduced to a four parameter problem, in Eqs. (20) and (21). These four parameters are listed as follows:

(i) Aspect ratio $s = h_1/b$ (for building 1).
(ii) The height ratio $\varepsilon = h_2/h_1$ (building 2 to 1).
(iii) The normalised inter-building distance ratio z (ratio of the distance between buildings to building width).
(iv) the soil class, that is defined using c_1, c_2, $\overline{V}_s$, ρ_s and μ (see Table 1).

2.3. Defining system performance measures

As a measure of change in the response between the coupled (SSSI) and uncoupled (SSI) systems, in this study we will use the following performance measures,

$$U_{2j} = u_{2j} - 3\frac{h_j}{b}\theta_j,\quad A_{2j} = \ddot{u}_{2j} + \ddot{u}_g - 3\frac{h_j}{b}\ddot{\theta}_j \tag{22}$$

where U_{2j} and A_{2j} are respectively the relative (sway + rotational) displacements and total (sway + ground + rotational) accelerations for the top of buildings "j" in non-dimensional form. So, U_2 and U_4 are the displacements at the top of buildings one and two. The error in the response total power, when using uncoupled SSI analyses rather than coupled SSSI analyses is defined as follow,

$$\chi_{ii} = 100\frac{[E_s(U_i)]_{SSSI} - [E_s(U_i)]_{SSI}}{[E_s(U_i)]_{SSI}} \tag{23}$$

where subscript i is from 1 to 4 and $E_s(U_i)$ is the total power spectral density (which is based on all data points of response timeseries U_i), which is defined using the Parseval's theorem according to Eq. (24).

$$E_s(U_i) = \int_{-\infty}^{\infty} |U_i(\tau)|^2 d\tau = \frac{1}{2\pi}\int_{-\infty}^{\infty} |U_i(\omega)|^2 d\omega \tag{24}$$

where $U_i(\omega)$ is the continuous Fourier transform of $U_i(\tau)$. This error/difference term χ_{ii} would be zero if there is no difference between SSSI and SSI analyses; thus, indicating no inter-building coupling effects. Therefore, χ_{ii} could be viewed as the error in not employing SSSI analyses for a coupled building configuration. χ_{22} is the error in the top displacement of building 1, and χ_{44} is the error for the top displacement of building 2.

Using the total power as a comparative metric delivers a statistical estimate of magnitude that is more robust than employing a single peak of the function. To obtain the uncoupled system response (SSI) case either (i) increase inter-building distance z to a very large value or (ii) set $q_\kappa = 0$ and $q_2 = 1$. Similarly, the error/difference in acceleration responses are defined as,

$$\ddot{\chi}_{ii} = 100\frac{[E_s(A_i)]_{SSSI} - [E_s(A_i)]_{SSI}}{[E_s(A_i)]_{SSI}} \tag{25}$$

Additionally, for a more forensic exploration of system responses used later, we define the norms of the system transfer functions. In frequency domain system analysis [40], we can determine the system response through the displacement transfer function $\mathbf{v}(\omega)$ between the degrees of freedom u_j and the earthquake $\ddot{u}_g$. By taking a Fourier transform of Eq. (11) we re-express the set of differential equations with a set of algebraic equation, thus,

$$\mathbf{U}(\omega) = \mathbf{v}(\omega)\ddot{U}_g(\omega),$$
$$\mathbf{v}(\omega) = -(\mathbf{K} + i\omega\mathbf{C} - \omega^2\mathbf{M})^{-1}\mathbf{p} = [v_1(\omega), ..., v_6(\omega)]^T \tag{26}$$

where the vector $U(\omega)$ is the Fourier transform of vector $\mathbf{u}(\tau)$, $\ddot{U}_g(\omega)$ is

the Fourier transform of the ground acceleration $\ddot{u}_g(\tau)$, and ω is the Fourier frequency. This can be expressed as the norm of the transfer function for the building 1 and 2.

$$\|\mathbf{v}_{b1}(\omega)\|_2 = \sqrt{v_1^2 + v_2^2 + v_3^2}, \quad \|\ddot{\mathbf{v}}_{b1}(\omega)\|_2 = \|(i\omega)^2\mathbf{v}_{b1}(\omega)\|_2$$
$$\|\mathbf{v}_{b2}(\omega)\|_2 = \sqrt{v_4^2 + v_5^2 + v_6^2}, \quad \|\ddot{\mathbf{v}}_{b2}(\omega)\|_2 = \|(i\omega)^2\mathbf{v}_{b2}(\omega)\|_2 \tag{27}$$

where $\|\mathbf{v}_{b1}(\omega)\|_2$ and $\|\mathbf{v}_{b2}(\omega)\|_2$ are the Euclidian norms of displacement response transfer functions for building 1 and 2 respectively. The acceleration transfer function is equal to $\ddot{\mathbf{v}}(\omega) = (i\omega)^2\mathbf{v}(\omega)$. Similarly, $\|\ddot{\mathbf{v}}_{b1}(\omega)\|_2$ and $\|\ddot{\mathbf{v}}_{b2}(\omega)\|_2$ are the Euclidian norms of acceleration response transfer functions for building 1 and 2 respectively. Thus, we shall employ:

(i) difference/error in total power responses, (Eqs. (23) and (25)) as an overall system comparative metric.
(ii) the Euclidian norms of response transfer functions (Eqs. (26) and (27)) for a more forensic system examination metric.

3. Analyses

3.1. Ground motion selection

To determine the effect of SSSI on the system we consider three types of ground motion. This includes Far-Field (FF), Near-Field Without Pulse (NFWP) and Near-Field Pulse-Like (NFPL) record sets [41]. The earthquakes that occur in fields close to a ruptured fault can have different characteristics than those further away from the seismic source. The Near-Field zone is a set of ground motions recorded at sites located less than 10 km from the fault rupture, and the Far-Field zone is to be at sites greater than 10 km from the fault rupture [35]. A pulse-like ground motion is considered to be a record with a short-duration pulse that occurs early in the velocity time history and has large amplitude [42]. One cause of these velocity pulses are forward-directivity effects in the near-fault region.

The ground motions database is obtained from FEMA P695 [35], which includes records with different characteristics, i.e. FF, NFPL and NFWP (see Fig. 2). The recorded acceleration series of these ground motions are selected from the Pacific Earthquake Engineering Research (PEER-NGA) West database [41]. The FEMA P695 recommends a set of 22 FF records that are taken from 14 events that occurred between 1971 and 1999. Eight of them occurred in California, and six of them are taken from different places around the world. Each record has two horizontal components. Event magnitudes range from $M_w = 6.5$ to $M_w = 7.6$ with an average magnitude of $M_w = 7.0$. Values of their peak ground accelerations (PGAs) vary from 0.21 g to 0.82 g with a mean value of 0.43 g.

3.2. Response of the system for a set of parameters

The analysis is carried out first for the Near-field Pulse-Like Loma Prieta earthquake for a selected combination of parameters as a starting example. We examine the case when the two buildings are placed in very close proximity to each other, i.e. at a spacing distance of $0.1b$ and hence $z = 0.1$. This building spacing has been demonstrated to be large enough to avoid pounding but close enough to maximise the SSSI effects [22–24,28]. The rigid base frequency of the building 1 is $\omega_{rb1}/2\pi = 3.3$ Hz. Then, in Sections 3.3 and 3.4, the three types of ground motion sets are considered, and a broader range of system parameters are explored.

An important feature of the SSSI systems is that the fundamental frequencies of the coupled system do not change very much compared to the uncoupled system, i.e. there is a maximum of 9% variation in the natural frequencies between the SSI and SSSI systems. This characteristic can be seen in the changes of peaks for the transfer functions, between the uncoupled and coupled system, in the following figures.

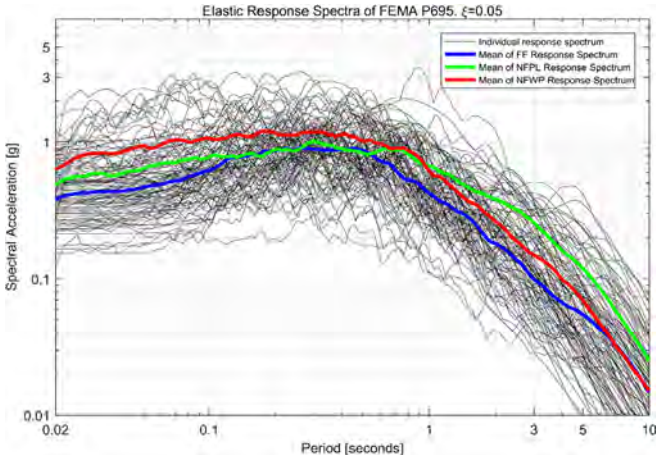

Fig. 2. Elastic response spectra of FEMA P695 ground motions.

Fig. 3(a) shows the uncoupled SSI (blue[1] line) and coupled SSSI (red line) response for the upper DOFs of the buildings 1 (namely the displacement U_2 and the total acceleration A_2). This is for the case where the second building is 10% taller than building 1, and building 1 has a height to width ratio equal to 2.6 (height ratio $\varepsilon = h_2/h_1 = 1.1$ and aspect ratio $s = h_1/b = 2.6$). Comparing the SSI and SSSI responses, we observe that the maximum displacement of buildings increases, when the coupling is considered, as well as total acceleration in almost all the time-history. Fig. 3(b) shows the corresponding power spectral density for the displacements and total acceleration for the building 1 considering the uncoupled and coupled case. Comparing the SSSI and SSI responses, we observe that building 1 is significantly affected by the taller building 2. There are big amplifications in the displacement and acceleration power spectral density for a Fourier frequency equal to 2.2 Hz (which mainly represents the building 1's first natural frequency). Building 1's displacement response power increases by $\chi_{22} = 78\%$ (change defined in Eq. (23)), and the system has a larger amplification in acceleration response power of $\ddot{\chi}_{22} = 120\%$ (change defined in equation (25)). In general, greater amplifications are observed for accelerations than for displacements, for height ratios close to 1.1.

Fig. 3(c) displays the norm transfer function for the displacements $\|\mathbf{v}_{b1}(\omega)\|_2$ and accelerations $\|\ddot{\mathbf{v}}_{b1}(\omega)\|_2$ for building 1. Comparing the uncoupled (blue line) and coupled case (red line) responses, there is a transfer of earthquake energy between building 2 (represented as the first peak in Fig. 3(d) with a Fourier frequency of 1.8 Hz) to building 1 (represented as the first peak in Fig. 3(c) with a Fourier frequency of approximately 2.2 Hz). The higher modes of the system do not produce a significant change in the response of the system, for height ratios close to 1.1 (buildings of similar height). Fig. 3(d) displays the norm transfer function for the displacement $\|\mathbf{v}_{b2}(\omega)\|_2$ and acceleration $\|\ddot{\mathbf{v}}_{b2}(\omega)\|_2$ for building 2. There is a decrease of energy in building 2 which produces a reduction in the response of $\chi_{44} = -45.2\%$ and $\ddot{\chi}_{44} = -16.7\%$ in the displacement and acceleration respectively. This is mainly due to the decrease in the first peak, coupled SSSI case. These Fig. 3(d) displays a classical tuned mass damper (TMD) characteristic, where building 1 can be viewed as a TMD for building 2.

Fig. 4 displays the response for a system that the second building is 2.5 times the first building, and building one has a height to width ratio equal to 2.6 (aspect ratio $s = h_1/b = 2.6$ and height ratio $\varepsilon = h_2/h_1 = 2.5$). Fig. 4(a) shows the uncoupled and coupled responses for the upper DOFs of building 1, that is the displacement U_2 and the total acceleration A_2. Comparing the uncoupled and coupled responses,

[1] For interpretation of color in Figs. 3, 6 and 7, the reader is referred to the web version of this article.

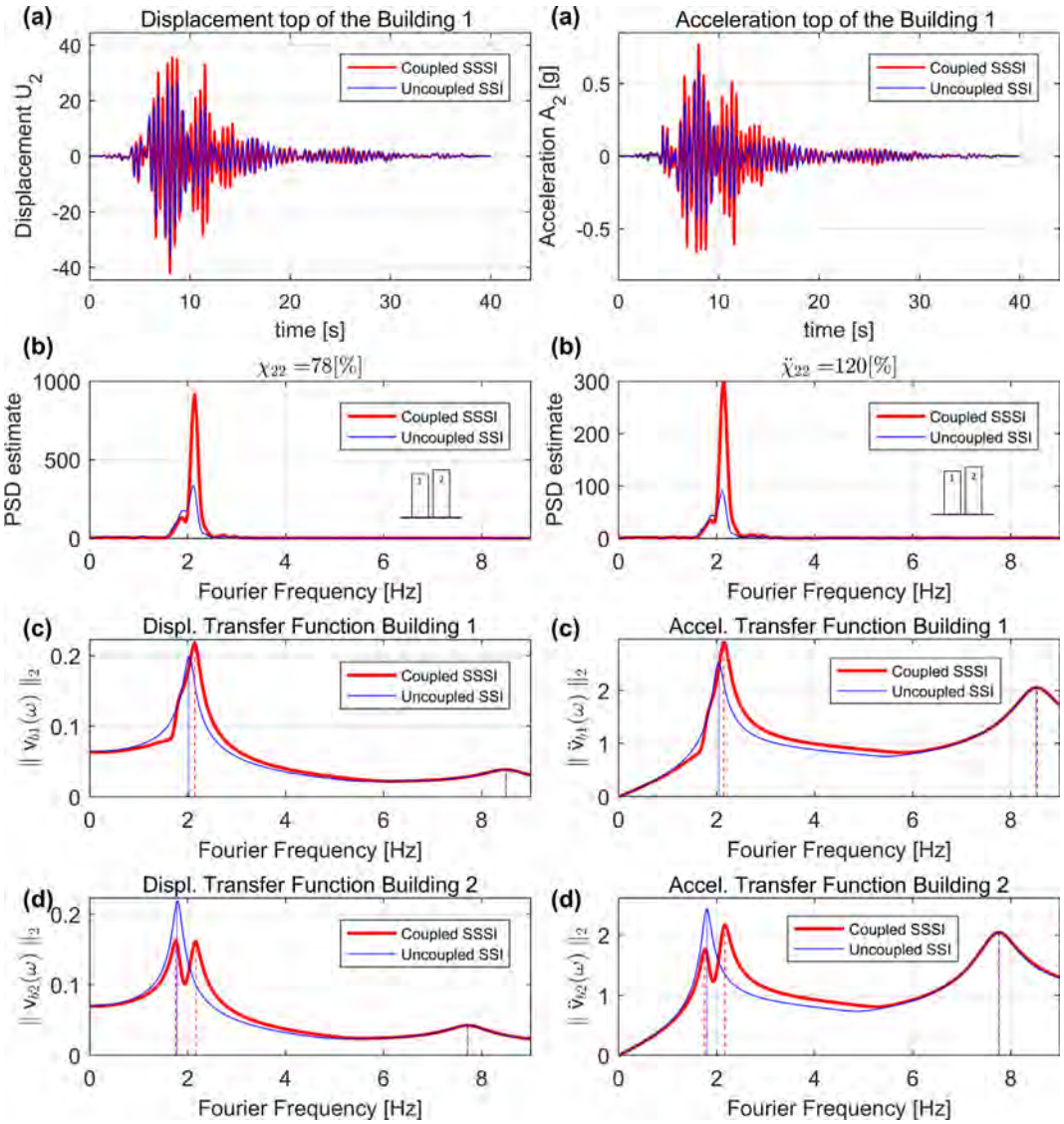

Fig. 3. Response on loose soil for parameter set ($\varepsilon = h_2/h_1 = 1.1$, s = $h_1/b = 2.6$, z = 0.1) (a) Displacement and acceleration responses. (b) Power spectral density of displacement and acceleration responses. (c) Transfer function for building 1. (d) Transfer function for building 2.

we observe that the maximum displacement and acceleration of buildings increases for the SSSI case, just like in the initial example.

Fig. 4(b) shows the power spectral density for the displacements and total accelerations. We observe that building 1′s total response power increase about χ_{22} = 63.7% and $\ddot{\chi}_{22}$ = 51.3% in the displacement and acceleration respectively. In general, for height ratios greater than 2.0, higher amplifications are observed for displacement than for acceleration. The main difference observed with the previous case is that there are 3 closely spaced resonances/modes (see Fig. 4(b)) as opposed to 2 closely spaced resonances/modes in the previous case of Fig. 3(b).

There is a significant amplification in the displacement power spectral density for a Fourier frequency equal to 0.61 Hz. This is mainly due to building 2′s first uncoupled natural frequency. As stated previously, the eigenfrequencies for the coupled and uncoupled system are very similar. However, the eigenmodes are different for the coupled system as they span the two buildings rather than a single building in the uncoupled system. The resonance at 0.61 Hz is not significant for acceleration, mainly because the acceleration response is not as susceptible to low-frequency content by definition. This is a result of the Eulerian relationship $\ddot{\mathbf{v}}(\omega) = (i\omega)^2\mathbf{v}(\omega)$. The second resonance in the displacement and acceleration occurs at a Fourier frequency equal to 2.1 Hz (which corresponds to building 1′s first uncoupled natural frequency). While the third resonance is due to building's 2 s uncoupled natural frequency.

Fig. 4(c) and (d) displays the norm of the transfer function for the displacement and acceleration for building 1 and 2 respectively. As in the previous case (Fig. 3), there is a transfer of earthquake energy between building 2 to building 1, producing a reduction in building 2′s responses of χ_{44} = −12.3% and $\ddot{\chi}_{44}$ = −4.1% in the displacement and acceleration respectively. For this parameter setting, the 'first modal frequency' of building 1 (represented by the second peak with a Fourier frequency of 2.1 Hz) is close to the natural frequency of the second mode in building 2 (represented by the third peak in Fig. 4(d) with a Fourier frequency of 3.4 Hz). This produces an additional amplification in the response of building 1.

To quantify the effect of secondary modes of building 2 on building

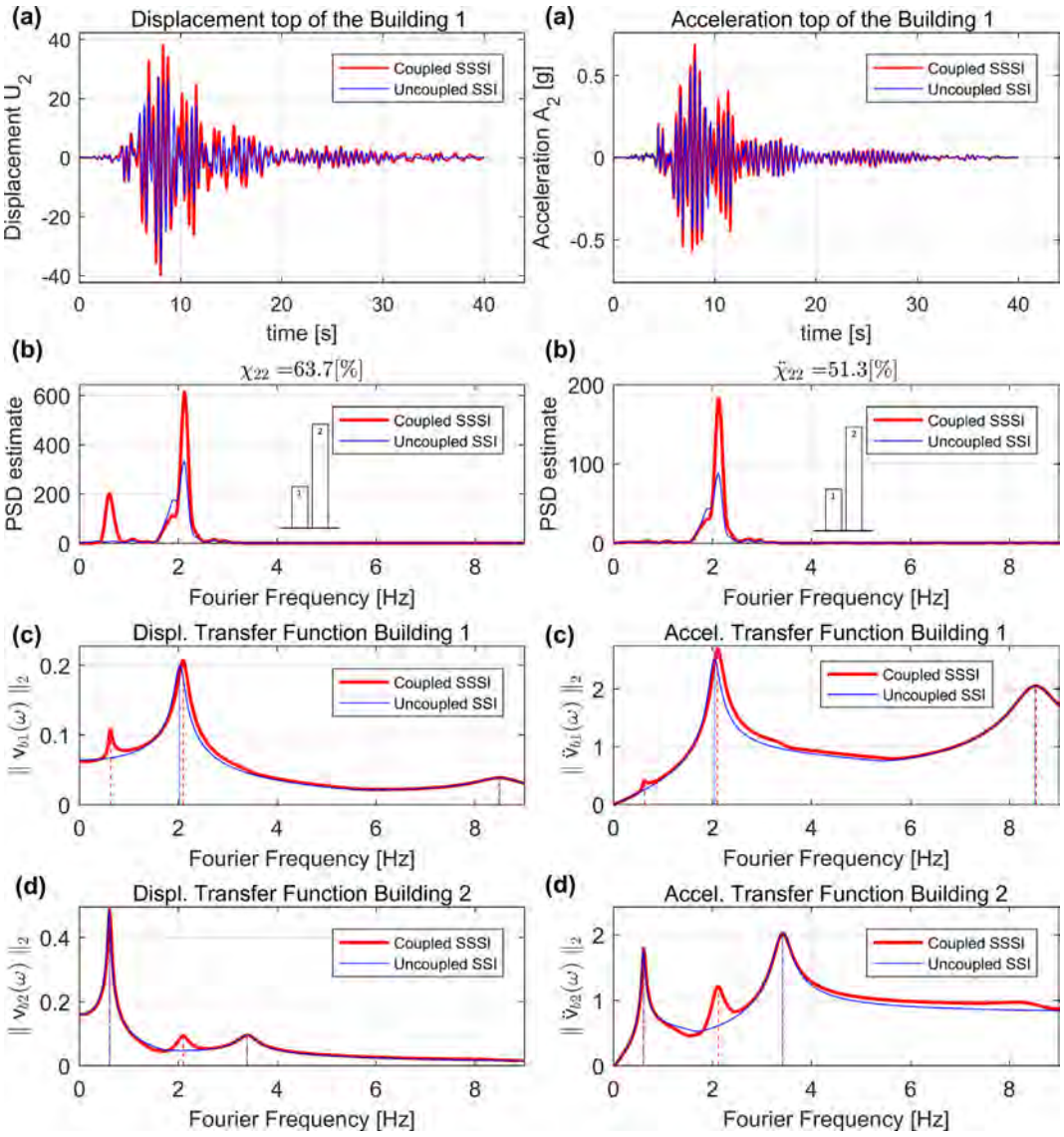

Fig. 4. Response on loose soil for parameter set ($\varepsilon = h_2/h_1 = 2.5$, $s = h_1/b = 2.6$, $z = 0.1$) (a) Displacement and acceleration response, (b) Power spectral density of displacement and acceleration responses, (c) Transfer function for building 1 and (d) Transfer function for building 2.

1, the response for the equivalent system described in the paper [22] will be calculated. This model represents a pair of buildings with 2 DOFs each, whose response is shown in Fig. 5. The main feature that differentiates the two models is that the reduced order model presented in this research allows the interaction between the second sway mode of the taller building with the first sway mode of the smaller building. This additional interaction it was not explored in the papers [22,23].

Fig. 5 shows the uncoupled and coupled response (system with original 4 dofs model [22]) when the second building is 2.5 times the first building, and the building one has a height to width ratio equal to 2.6. In this case, building 1's total response power increase about $\chi_{11} = 20\%$ and $\ddot{\chi}_{11} = 24.6\%$ in the displacement and acceleration respectively, versus the values $\chi_{22} = 63.7\%$ and $\ddot{\chi}_{22} = 51.3\%$ shown in Fig. 4(b). This difference is mainly due to the additional degree of freedom in each building, and it generally occurs when the first natural frequency of building 1 is close to the second natural frequency of building 2. This is likely to occur if the height ratio between the two buildings is greater than 2. In addition, in Fig. 5(c) we can observe that the third and fourth peak disappeared. So, amplification/reduction in the response is only influenced by the first two modes. Thus, adding an extra degree of freedom to building 1 and 2 may increase the interaction between the buildings. Nevertheless, incorporating further additional degrees of freedom into the buildings (i.e. greater than 3 DOF per building) does not significantly affect the SSSI system response. This is because the modal participation factors of additional higher system modes are very small.

For some specific ground motion, there is a significant amplification in displacement when the height ratios are greater than 2.0. Fig. 6(a) shows the response for the Near-field Pulse-Like Erzicam ground motion. Comparing the SSI and SSSI responses, there is a large amplification in the displacements $\chi_{22} = 258\%$ but not in accelerations $\ddot{\chi}_{22} = 18.6\%$. Fig. 6(b) displays the norm of the transfer function for each degree of freedom corresponding to building 1. It is seen that the amplification in displacement comes through the amplification of the rotation/rocking of building 1, due to the presence of the taller building 2. The taller building has a fundamental modal frequency at 0.8 Hz

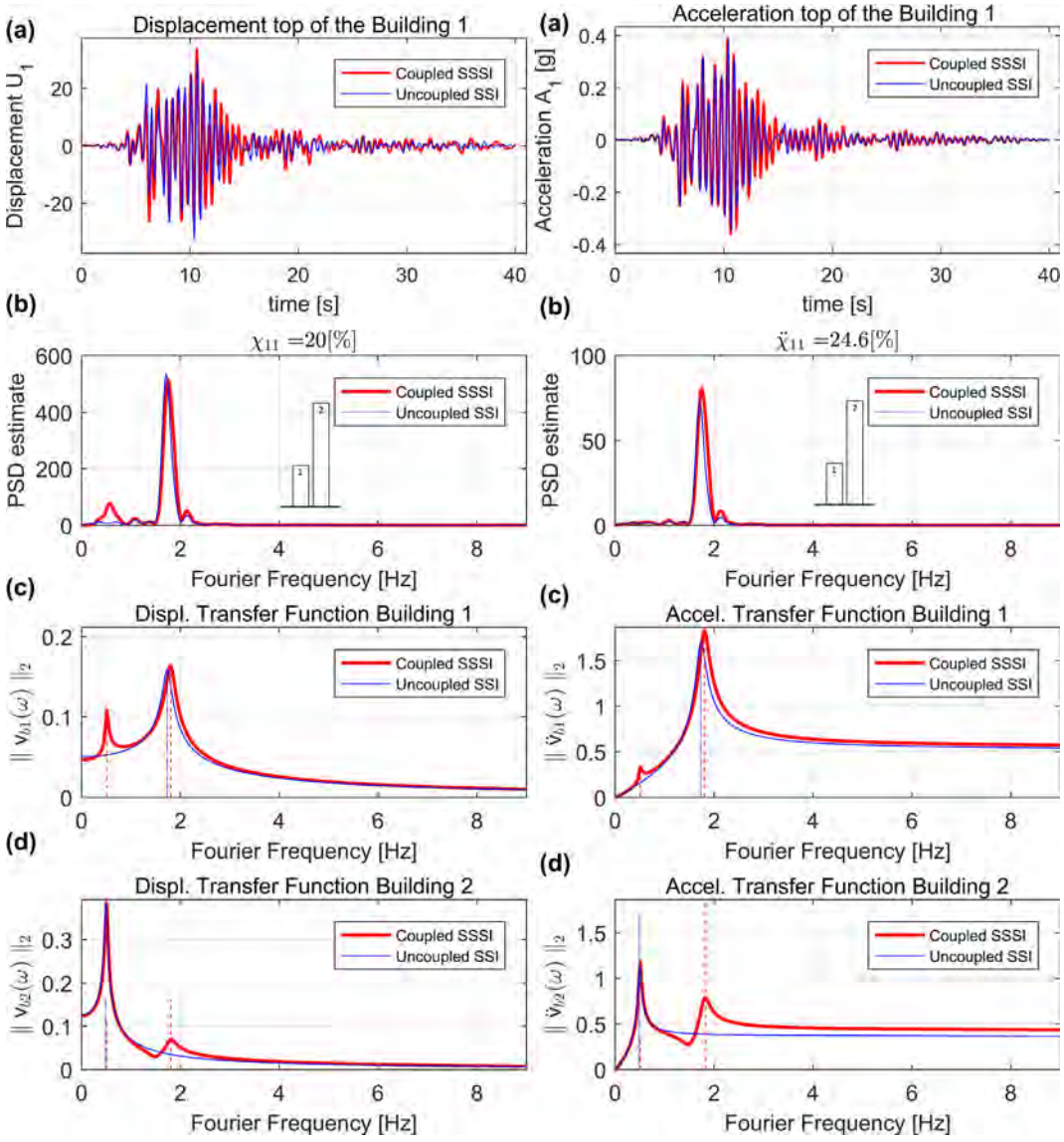

Fig. 5. Response on loose soil for parameter set ($\varepsilon = h_2/h_1 = 2.5$, $s = h_1/b = 2.6$, $z = 0.1$) (a) Displacement and acceleration response for a system with 4 dofs, (b) Power spectral density, (c) Transfer function for building 1 and (d) Transfer function for building 2.

when it is uncoupled. In the coupled system, this 0.8 Hz mode, remains at approximately 0.8 Hz, but has an eigenvector (spanning the entire couple system) with a large rotational component in building 1. Thus, we observe very large differences in displacement responses from SSI and SSSI analyses for this case. The taller building seems to induce a large 'rigid body rocking' in the smaller building, which is represented by the peak (at 0.8 Hz) in the transfer function for the rotation of building 1 (red line).

This behaviour is not observed for the acceleration responses because all low-frequency acceleration responses are not subjected to low-frequency amplification. This is a result of the Eulerian relationship $\ddot{\mathbf{v}}(\omega) = (i\omega)^2\mathbf{v}(\omega)$.

3.3. Change in power with variation in aspect ratio ε and height ratio s

We now take a look at the error in total power of building 1, defined in Eq. (23) for the displacement $\chi_{22}(s, \varepsilon)$ and defined in Eq. (25) for the acceleration $\ddot{\chi}_{22}(s, \varepsilon)$. This error/difference term would be zero if there is no difference between the coupled (SSSI) and uncoupled (SSI) analyses.

The variation of error in power, with height $\varepsilon = h_2/h_1$ and aspect ratio $s = h_1/b$ for loose soil and inter-building spacing of $z = 0.1$, is plotted. Again, noting that this inter-building spacing is validated in [22–24]. The system is subjected to all earthquake events, classified by Far-Field (FF), Near-Field Without Pulse (NFWP) and Near-Field Pulse-Like (NFPL) record sets. For each of these record sets, the maximum of maxima error (for this record set), the mean error (for this record set) and the standard deviation of error (for this record set) are presented.

Fig. 7(a) displays the contour plots of variation of error $\chi_{22}(s, \varepsilon)$ for the displacement U_2 on top of building 1, for the Far-Field records. Fig. 7 contains the results of nearly half million different time-histories analyses. We employed University of Bristol's supercomputer, BlueCrystal, for these simulations. The critical zones in the figure are red, i.e. where the total response power of building 1 is amplified by the

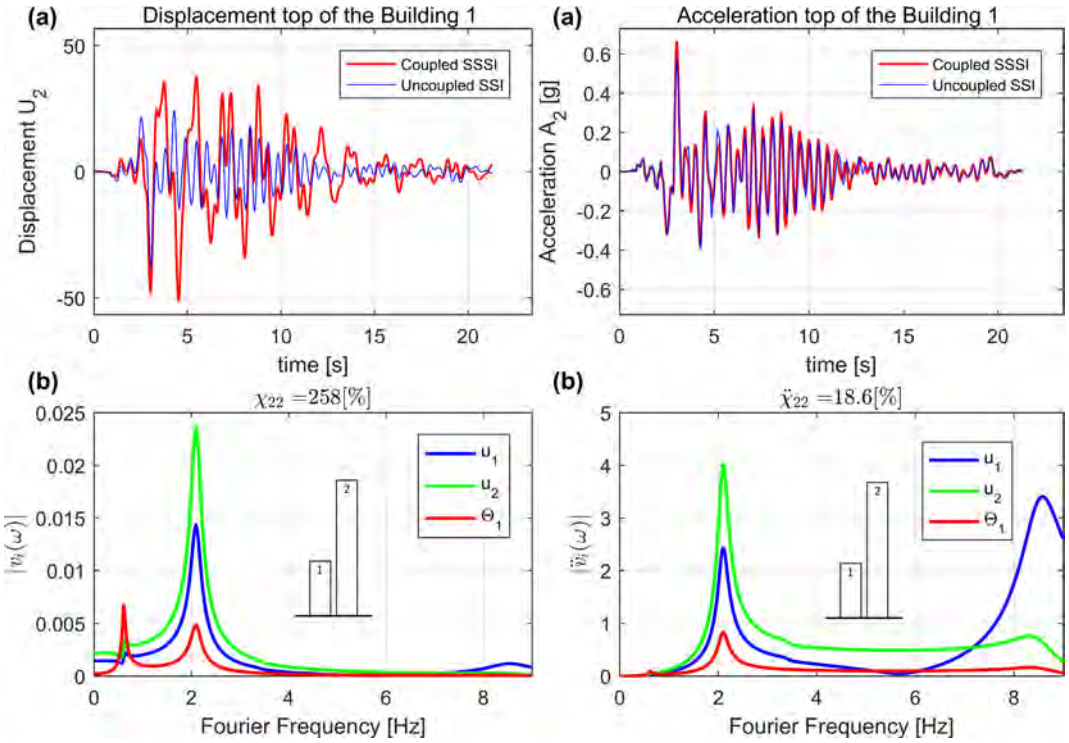

Fig. 6. Response on loose soil for parameter set ($\varepsilon = h_2/h_1 = 2.5$, $s = h_1/b = 2.6$, $z = 0.1$) (a) Displacement and acceleration responses and (b) Transfer function for individual DOFS in SSSI case.

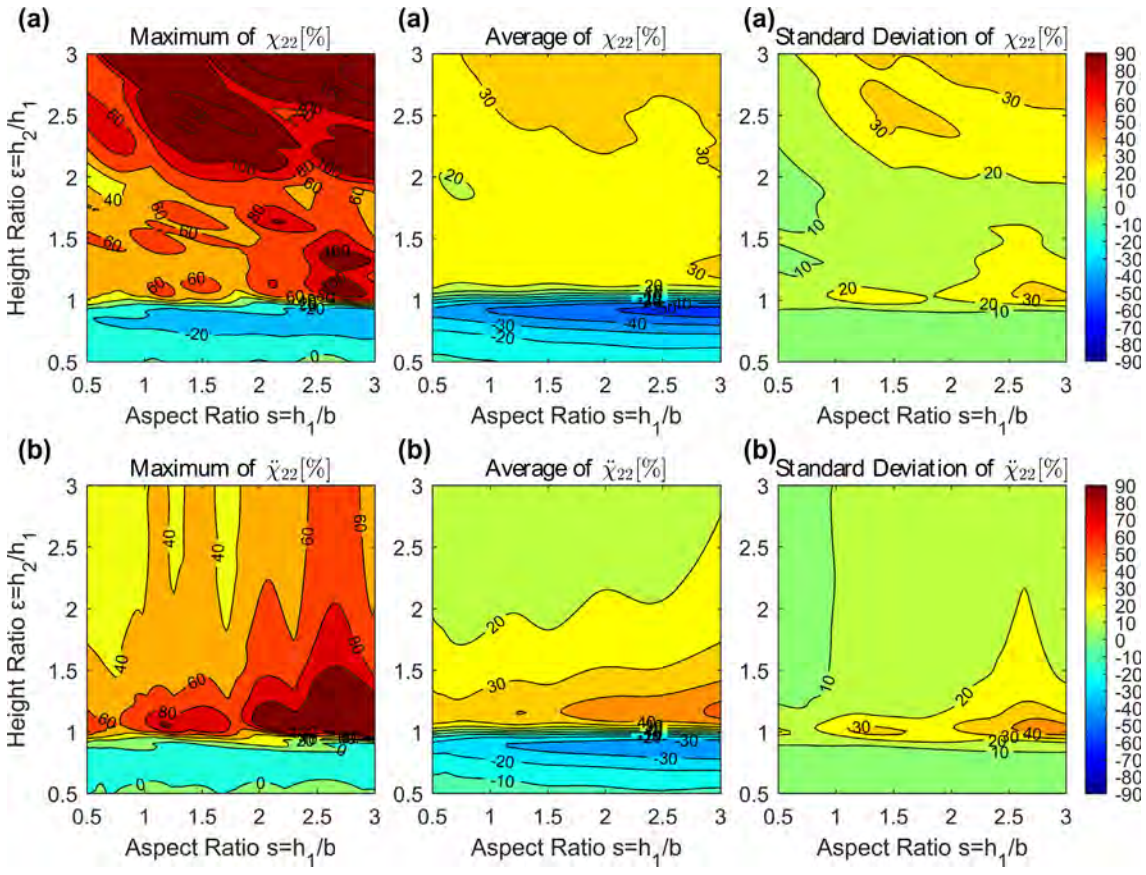

Fig. 7. Response on loose soil and $z = 0.1$ for Far-Field records. Maximum value, average and standard deviation for error in (a) displacement power $\chi_{22}(\boldsymbol{s}, \varepsilon)$ and (b) acceleration power $\ddot{\chi}_{22}(\boldsymbol{s}, \varepsilon)$.

presence of building 2. Blue indicates when the response power is reduced. With the aim of making the figure more readable, the change in the color contour is shown up to a value of 90%, and for larger values only the contour line is marked. For height ratios greater than 1, i.e. when adjacent buildings are taller, the response of building 1 is amplified. The maximum increase in total displacement power response occurred when the structure configuration lies around $\chi_{22}(2.6, 1.1) = 110\%$, and when the height ratio is greater than 2. On average, the amplification reaches a value of 20% and a standard deviation of 15%. Thus, a very similar trend is observed on the change in power for all FF earthquake for the whole range of parameters.

Fig. 7(b) displays the contour plots of variation of error in power $\ddot{\chi}_{22}(s, \varepsilon)$ (i.e. the error in using SSI analysis for a coupled building scenario) for the acceleration A_2, considering the top of building 1 and FF records. As with the displacement, for height ratios greater than 1 the response of building 1 is amplified. The maximum increase in total acceleration power response occurred when the building parametric configuration lies around $\ddot{\chi}_{22}(2.5, 1.1) = 110\%$ and its average is approximately $\ddot{\chi}_{22}(s, 1.1) = 40\%$. The dispersion of the values is small, with a maximum of 40%, for the whole range of analysed parameters.

Fig. 8(a) displays the contour plots of variation of error in power $\chi_{22}(s, \varepsilon)$ for the displacement U_2 considering the Near-Field Pulse-Like records. Again in Figs. 8 and 9 over half a million different time-histories analyses are developed. Unlike the Fig. 7(a), there is a large amplification when the height ratio is greater than 2.0, reaching values above 400% of amplification.

Fig. 8(b) displays the contour plots of variation of change in power $\ddot{\chi}_{22}(s, \varepsilon)$ for the acceleration A_2, for NFPL records. As with the FF records, the maximum increase in total acceleration power response occurred when the structure configuration lies around $\chi_{22}(2.6, 1.1) = 110\%$. The dispersion of the values is small, with a maximum of 30%, for the whole range of analysed parameters. However, unlike the results shown in Figs. 7(a) and 8(a), the variation of power for the acceleration decreases as the height ratio increases. This is because the response accelerations are not susceptible to low-frequency content, as shown in Fig. 4(b). On the other hand, the displacement responses are susceptible to low-frequency content, as exemplified by the peak produced in the power spectral density in Fig. 5(b), especially when the height ratio is greater than 2 (the taller building 2 produces a great influence on building 1).

Fig. 9 shows the variation of error in power for the displacement U_2 and acceleration A_2 considering Near-Field Without Pulse records. In general, the behaviour of NFPL and NFWP earthquakes follows a similar pattern for maximum values, averages and standard deviation. Comparing the FF and NF earthquakes, the contour plots suggest that the low-frequency content of the earthquake (especially for Near-Field records) can affect the size of adverse SSSI effects, especially for response displacements when the height ratio is greater than 2.0.

Fig. 10 depicts the power spectral density estimate of all earthquakes and the average for FF, NFPL and NFWP records sets. We can see that, on average, the NF records set has a larger average low-frequency content (between Fourier frequency 0.01 Hz to 1 Hz). This larger low-

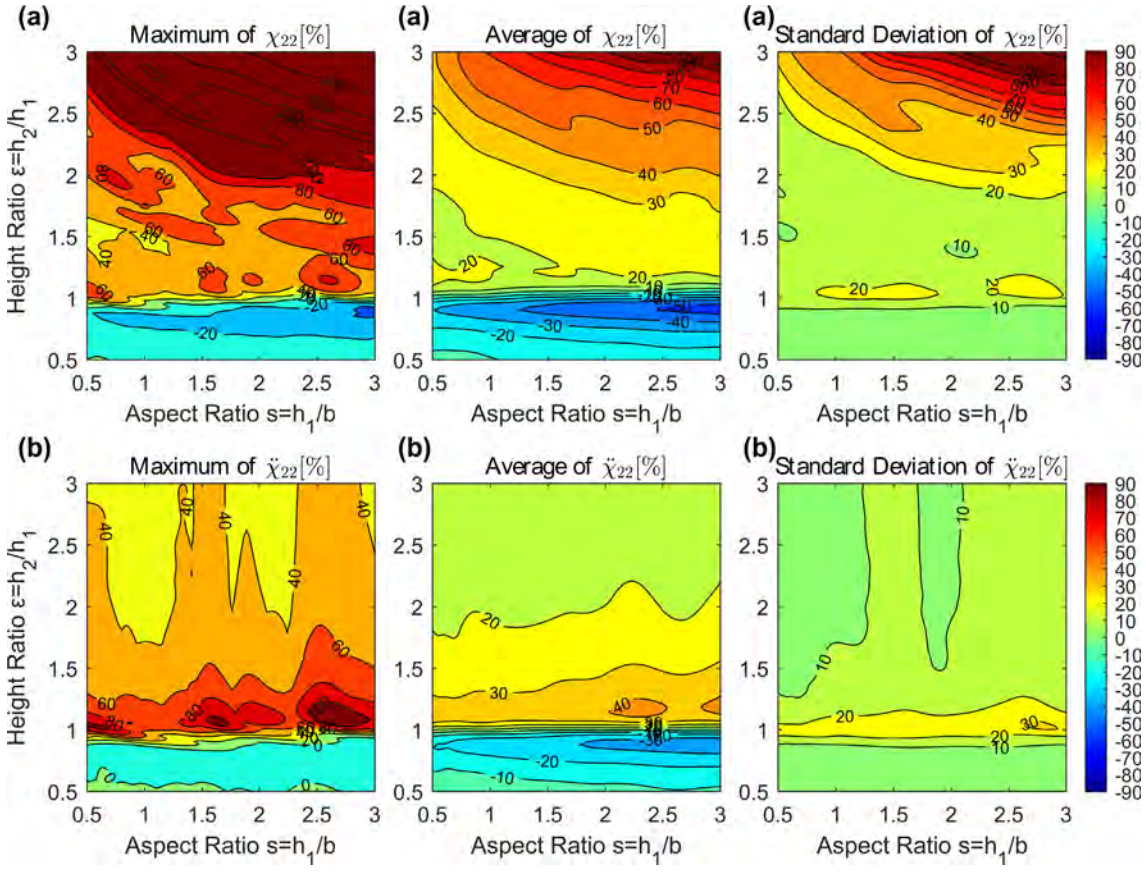

Fig. 8. Response on loose soil and z = 0.1 for Near-Field Pulse-Like records. Maximum value, average and standard deviation for error in (a) displacement power $\chi_{22}(\boldsymbol{s}, \varepsilon)$ and (b) acceleration power $\ddot{\chi}_{22}(\boldsymbol{s}, \varepsilon)$.

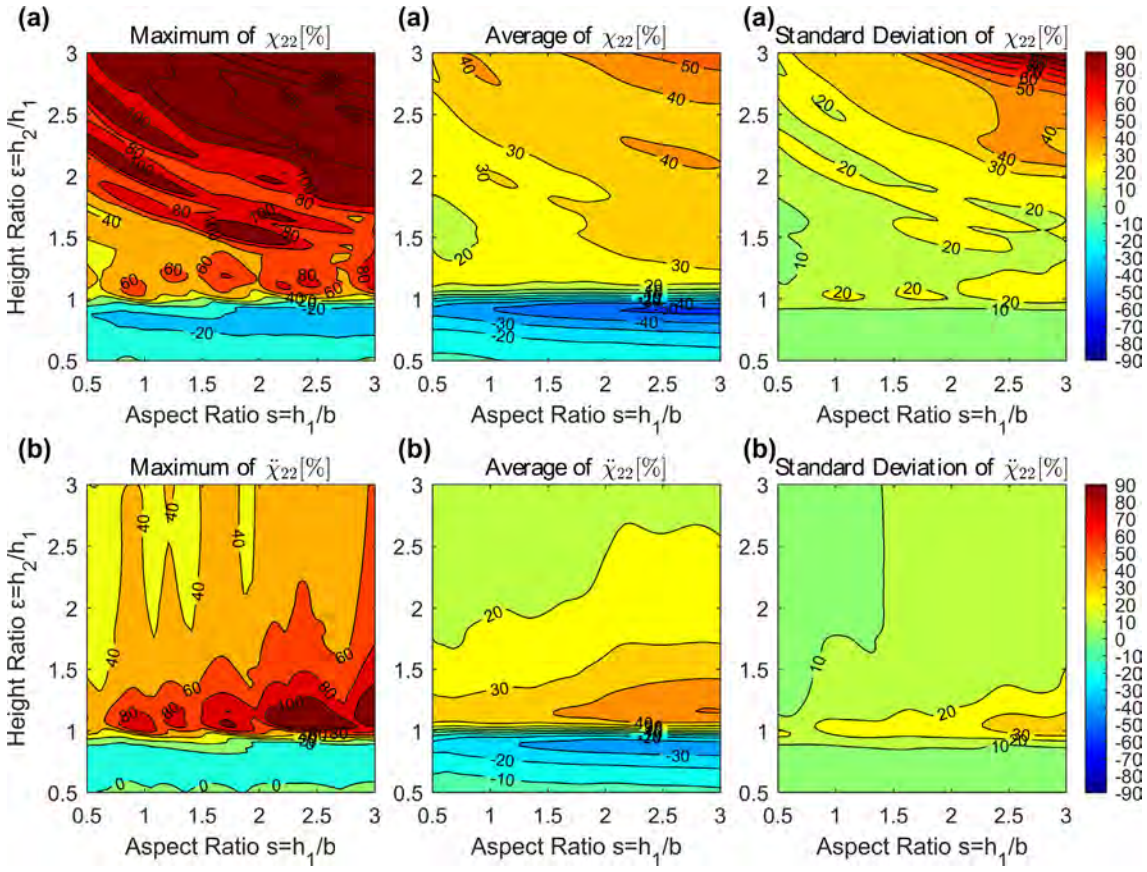

Fig. 9. Response on loose soil and z = 0.1 for Near-Field Without-Pulse records. Maximum value, average and standard deviation for error in (a) displacement power $\chi_{22}(\boldsymbol{s}, \varepsilon)$ and (b) acceleration power $\ddot{\chi}_{22}(\boldsymbol{s}, \varepsilon)$.

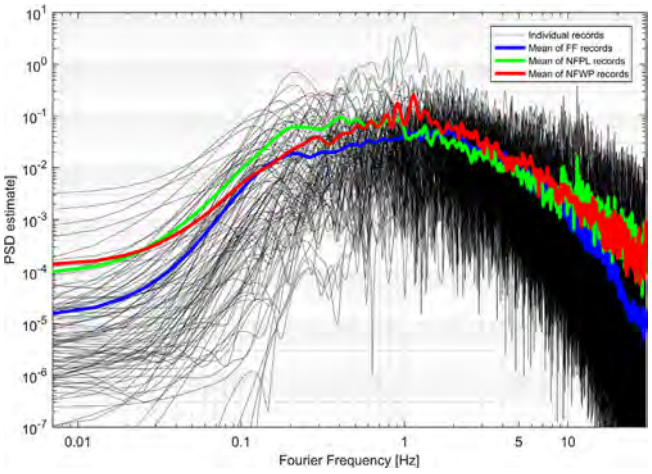

Fig. 10. Power spectral density estimate for ground acceleration records.

frequency content results in more significant responses in displacements (through a 'rigid body rocking' mode in the smaller building) when a small building is adjacent to a tall building.

3.4. Change in power due to variation in soil type and inter/building spacing z

Fig. 11 displays the previous analysis for the case of dense sand and the three types of ground motions plotted together. Figs. 11 and 12, contain more than 2 million different time-histories analyses. In this case, the amplification/reduction in the change of power are more limited, $\chi_{22}(2.6, 2.5) = 110\%$ and $\ddot{\chi}_{22}(2.8, 1.1) = 60\%$ in the displacement and acceleration respectively. Therefore, the worst seismic interaction condition occurs on loose soil as reported previously in [22–24].

Fig. 12(a) shows the variation of power $\chi_{11}(s, \varepsilon, z)$ for the displacement with height ratio $\varepsilon = h_2/h_1$ and inter-building spacing z, considering the three types of ground motions plotted together. The aspect ratio was set equal to $s = h_1/b = 2.0$. As expected, the effects of SSSI decreases when increasing the inter-building spacing, being practically negligible $\chi_{11}(2.0, \varepsilon, 2.0) = 3.5\%$ with a distance between foundations equal to $2b$. Fig. 12(b) repeats the previous analysis for the change in power $\ddot{\chi}_{11}(s, \varepsilon, z)$ in the acceleration and similarly, the interaction effect drops when increasing the inter-building spacing to a value of $\ddot{\chi}_{11}(2.0, \varepsilon, 2.0) = 2.8\%$.

4. Conclusion

In this paper, we present a theoretical formulation, which is a reduced order model, for Structure-Soil-Structure interaction between

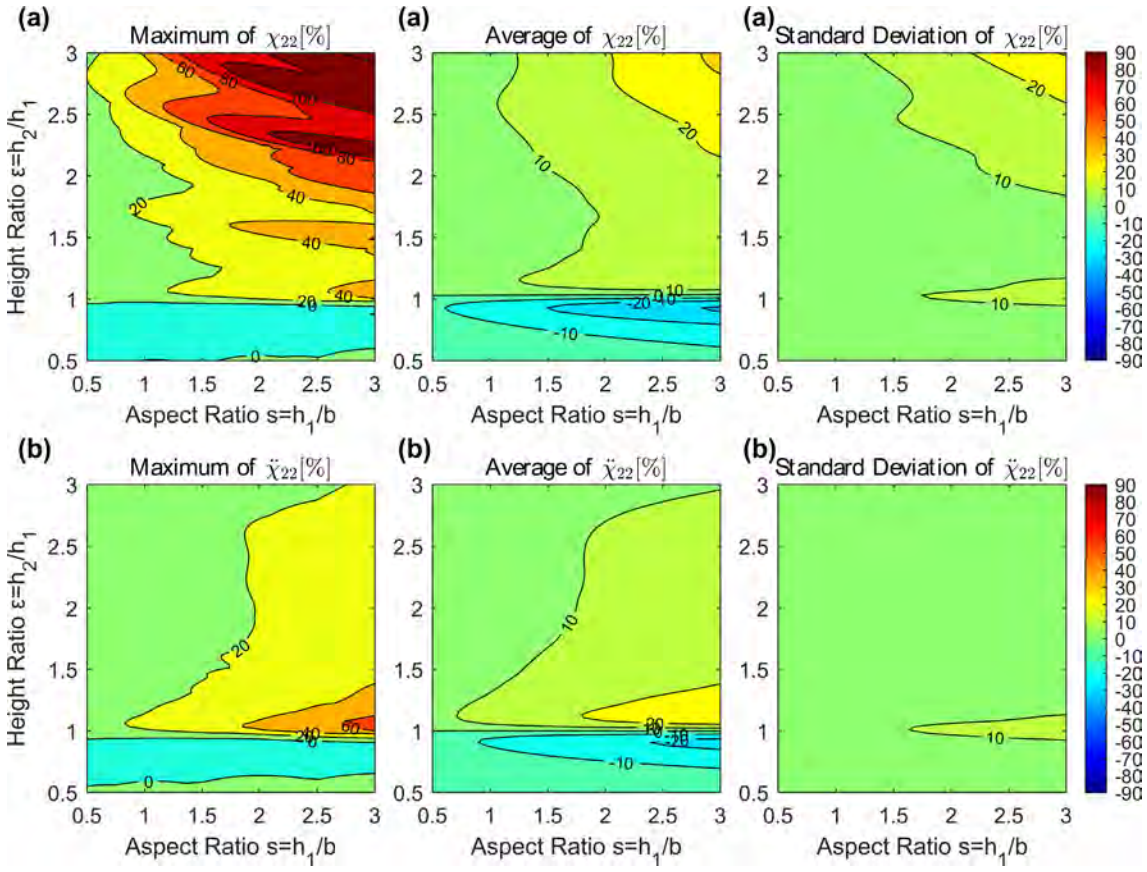

Fig. 11. Response on dense soil and z = 0.1 under all ground motion records. Maximum value, average and standard deviation for error in (a) displacement power $\chi_{22}(\boldsymbol{s}, \varepsilon)$ and (b) acceleration power $\ddot{\chi}_{22}(\boldsymbol{s}, \varepsilon)$.

two buildings that are coupled through the soil. Three types of ground motion were considered (Far-Field, Near-Field Without Pulse and Near-Field Pulse-Like records sets), selected from FEMA P695. It is shown that the complexity of the analysis is high due to a large number of system parameters, even for this reduced order model. Hence, a series of reasonable assumptions have been made to reduce further the number of system parameters. The parametric exploration undertaken in this paper explores the system response behaviour for a large range of buildings, inter-building spacing, soil types as well as ground motion excitation. These dynamic simulations involve over 3.1 million unique time-history analyses. It should be noted that the reduced order SSSI model was previously calibrated and validated with (i) finite element analyses [22] (ii) physical experimental test using the University of Bristol's shaking table and University of Dundee's centrifuge [23,28,29] and (iii) an analytical formulation derived from a Boussinesq deformation field of an elastic half-space [24].

The linear SSSI parametric study showed that there are detrimental and beneficial configurations for the dynamic characteristics of buildings. Regardless of the earthquake event (FF, NFWP or NFPL), it is found that the effect of interaction is unfavourable for building 1 when building 2 is taller: i.e. the power of the earthquake passed from the taller structure to the smaller structure. For the displacement responses, there is an increase in the response of up to 400%, when there is a large difference of height (height ratio $\varepsilon = h_2/h_1 > 2.0$) between the buildings. This result was not observed in previous studies [22,23,28]. The taller building imposes a low-frequency 'rigid body rocking mode' on the smaller building. If this behaviour is combined with ground motions that have a larger low-frequency content (i.e. the near field records), then there is significant error in using SSI analyses rather than SSSI analyses for these cases. This behaviour is observed in displacement responses alone because acceleration responses are, by definition, much less susceptible to low-frequency excitation.

For the acceleration responses, the greatest amplifications, of up to 120%, are observed for height ratio approximately of $\varepsilon = h_2/h_1 = 1.1$ (i.e. buildings of 10% difference in height). This finding confirms the results of previous studies [22,23] with a 4dof model and artificial ground motion records.

Results also indicated that there is a beneficial geometric configuration ($\varepsilon = h_2/h_1 < 1.0$) where the seismic risk is reduced in building 1 by the presence of a smaller building 2. A maximum of reduction of -45% for displacement and acceleration is observed. Both adverse and beneficial effects diminish as (i) building spacing increase and as (ii) the soil stiffness increases.

Results obtained from this 6dof model suggest that the introduction of two additional DOFs (i.e. enlarging 4dof model [22,23] to 6dof model developed here) can affect the size of interaction between the buildings. In this case, the 6 dof model permits the interaction of the second sway mode of a much taller building with the first sway mode of a shorter building of less than half its height. This indicates modal coupling is possible between more than just the primary modes of each

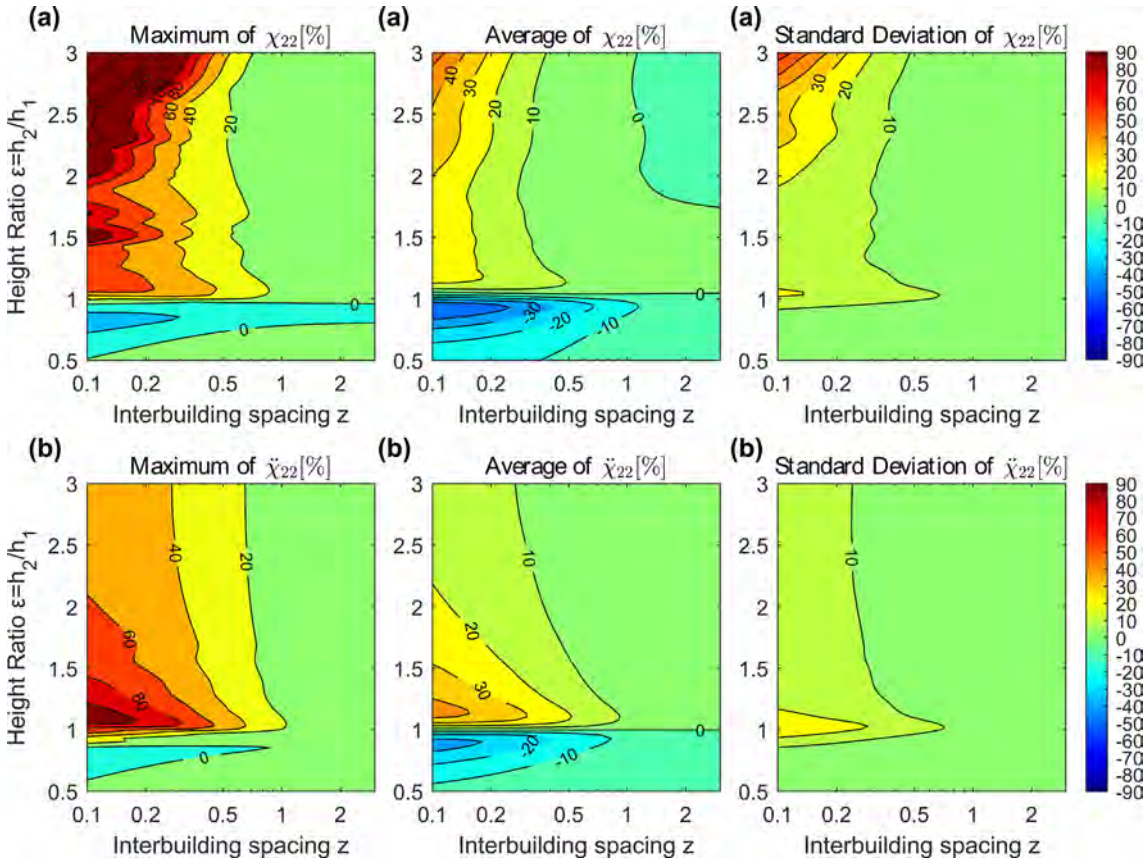

Fig. 12. Response on loose soil and aspect ratio s = 1.0 for all ground motion records. Maximum value, average and standard deviation for error in (a) displacement power $\chi_{22}(\boldsymbol{s}, \varepsilon, \boldsymbol{z})$ and (b) acceleration power $\ddot{\chi}_{22}(\boldsymbol{s}, \varepsilon, \boldsymbol{z})$.

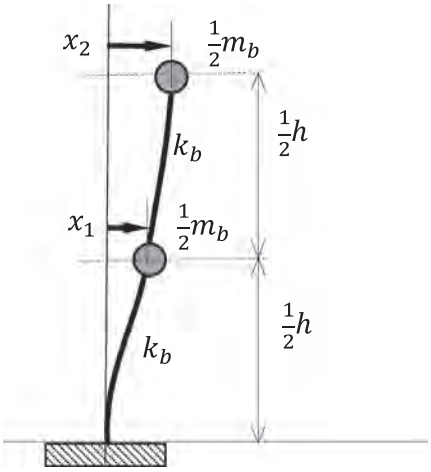

Fig. 13. Idealised two degree of freedom model.

building and therefore suggests a significant interaction between a taller building 1 and much shorter building 2. This result cannot be observed in the 4dof model where the most significant interactions occur when the buildings heights are within 10% of each other [22,23].

This raises the question as to whether there is a possible interaction between first and third building sway modes, second and third building sway modes, etc. Mathematically, these interactions are permissible with a reduced order model that has a sufficiently large number of DOFs and an appropriate set of system parameters. However, it should be noted that these interactions are likely to be less significant because the modal participation factors for higher modes is much smaller than for the primary modes.

Finally, there is evidence to suggest that the ground motion type can affect linear SSSI behaviour. The SSSI displacement responses do not follow the same trend as acceleration responses, and the introduction of the higher mode model does help to capture the SSSI behaviour in the case of a small building adjacent to a tall building.

Acknowledgements

The Ministry of Education, Chile and Commission for Scientific and Technological Research (CONICYT) through grant BCH 72170305 has granted financial support to the PhD student during this research. The researchers are very grateful for the support of the Faculty of Engineering, at the University of Bristol. Most of the computations necessary for this work were carried out on the BlueCrystal super-computers of advanced computing research centre of the University of Bristol.

Appendix A. Theoretical formulation of rigid base building

Fig. 13 shows a two degree of freedom system x_1 and x_2, where it is considered a rigid base foundation for the building. m_b is the total mass of the building, k_b is the building's stiffness and h is the total height of the building.

Hence, the stiffness and mass matrix of the 2-dof can be defined according to:

$$\frac{1}{2}m_b\begin{bmatrix}1 & 0\\ 0 & 1\end{bmatrix}\begin{bmatrix}\ddot{x}_1\\ \ddot{x}_2\end{bmatrix} + k_b\begin{bmatrix}2 & -1\\ -1 & 1\end{bmatrix}\begin{bmatrix}\boldsymbol{x}_1\\ \boldsymbol{x}_2\end{bmatrix} = 0 \Rightarrow \mathbf{M\ddot{x}} + \mathbf{Kx} = 0 \tag{28}$$

Through solving the resultant homogeneous eigenvalue problem $|\mathbf{K}-\omega\mathbf{M}| = 0$, we can obtain the first modal circular frequency, where the coefficient 0.874 is obtained through solving the eigenproblem's quadratic characteristic polynomial for the first root.

$$\omega_{\boldsymbol{rb}1} = 0.874\sqrt{\frac{\boldsymbol{k_b}}{\boldsymbol{m_b}}} \tag{29}$$

Appendix B. Summary of ground motions

Tables 2 and 3.

Table 2
Summary of Earthquake records for the Far-Field Records Set.

Record Name – Station	PGA [g]	M_w	Record Name – Station	PGA [g]	M_w
Northridge, USA – Beverly Hills	0.52	6.7	Landers, USA – Coolwater	0.42	7.3
Northridge, USA – Canyon Country	0.48	6.7	Loma Prieta, USA – Capitola	0.53	6.9
Duzce, Turkey – Bolu	0.82	7.1	Loma Prieta, USA – Gilroy Array #3	0.56	6.9
Hector Mine, USA – Hector	0.34	7.1	Manjil, Iran – Abbar	0.51	7.4
Imperial Valley, USA – Delta	0.35	6.5	Superstition Hills, USA – El Centro	0.36	6.5
Imperial Valley, USA – EC #11	0.38	6.5	Superstition Hills, USA – Poe Road	0.45	6.5
Kobe, Japan – Nishi-Akashi	0.51	6.9	Cape Mendocino, USA – Rio Overpass	0.55	7.0
Kobe, Japan – Shin-Osaka	0.24	6.9	Chi-Chi, Taiwan – CHY101	0.44	7.6
Kocaeli, Turkey – Duzce	0.36	7.5	Chi-Chi, Taiwan – TCU045	0.51	7.6
Kocaeli, Turkey – Arcelik	0.22	7.5	San Fernando, USA – LA Hollywood	0.21	6.6
Landers, USA – Yermo Fire Station	0.24	7.3	Friuli, Italia - Tolmezzo	0.35	6.5

Table 3
Summary of Earthquake records for the Near-Field Records Sets.

Record name NFPL – station	PGA [g]	M_w	Record name NFWP – station	PGA [g]	M_w
Imperial Valley, USA – El Centro #6	0.45	6.5	Gazli, USA – Karakyr	0.86	6.8
Imperial Valley, USA – El Centro #7	0.47	6.5	Imperial Valley, USA – Bonds Corner	0.78	6.5
Irpinia, Italy – Sturno	0.32	6.9	Imperial Valley, USA – Chihuahua	0.27	6.5
Superstition Hills, USA – Parachute	0.43	6.5	Nahanni, Canada – Site 1	1.20	6.8
Loma Prieta, USA – Saratoga	0.51	6.9	Nahanni, Canada – Site 2	0.52	6.8
Erzican, Turkey – Erzican	0.50	6.7	Loma Prieta, USA – Bran	0.50	6.9
Cape Mendocino, USA – Petrolia	0.66	7.0	Loma Prieta, USA – Corralitos	0.64	6.9
Landers, USA – Lucerne	0.79	7.3	Cape Mendocino, USA – C. Mendocino	1.49	7.0
Northridge, USA – Rinaldi Receiving	0.87	6.7	Northridge, USA – LA Sepulveda	0.93	6.7
Northridge, USA – Sylmar Olive View	0.84	6.7	Northridge, USA – Saticoy	0.46	6.7
Kocaeli, Turkey – Izmit	0.23	7.5	Kocaeli, Turkey – Yarimca	0.32	7.5
Chi-Chi, Taiwan – TCU065	0.79	7.6	Chi-Chi, Taiwan – TCU067	0.50	7.6
Chi-Chi, Taiwan – TCU102	0.30	7.6	Chi-Chi, Taiwan – TCU084	1.01	7.6
Duzce, Turkey – Duzce	0.51	7.1	Denali, Alaska – TAPS Pump Sta.	0.33	7.9

Appendix C. Supplementary data

Supplementary data associated with this article can be found, in the online version, at https://doi.org/10.1016/j.engstruct.2018.07.049.

References

[1] Luco JE, Contesse L. Dynamic structure–soil–structure interaction. Bull Seismol Soc Am 1973;63:1289–303.
[2] Kobori T, Minai R, Kusakab K. Dynamical characteristics of soil–structure cross-interaction system. Bull Disaster Prevent Res Inst 1973:22. [Kyoto University].
[3] Lee TH, Wesley DA. Soil–structure interaction of nuclear reactor structures considering through-soil coupling between adjacent structures. Nucl Eng Des 1973;24:374–87.
[4] Murakami H, Luco JE. Seismic response of a periodic array of structures. J Eng Mech, ASCE 1977;103(5):965–77.
[5] Wong HL, Trifunac MD. Two-dimensional, antiplane, building–soil–building interaction for two or more buildings and for incident planet SH waves. Bull Seismol Soc Am 1975;65:1863–85.
[6] Lysmer J, Seed HB, Udaka T, Hwang RN, Tsai CF. Efficient finite element analysis of seismic soil structure interaction. Report No. EERC 75-34. University of California (Berkeley, CA): Earthquake Engineering Research Center; 1975.
[7] Roesset JM, Gonzalez JJ. Dynamic interaction between adjacent structures. In: Proceedings of dynamical methods in soil and rock mechanics, Karlsruhe, September 5–16, 1977.
[8] Mattiesen PB, MacCalden RB. Coupled response of two foundations. In: Presented at the 5th world conference on earthquake engineering. Rome (Italy); 1974.
[9] Kobori T, Minai R, Kusakabe K. Dynamical cross-interaction between two foundations. In: Presented at the 6th world conference on earthquake engineering. New Delhi (India); 1977.
[10] Qian J, Beskos DE. Dynamic interaction between 3-D rigid surface foundations and comparison with the ATC-3 provisions. Earthq Eng Struct Dyn 1995;24:419–37.
[11] Betti R. Effects of the dynamic cross-interaction in the seismic analysis of multiple embedded foundations. Earthq Eng Struct Dyn 1997;26:1005–19.
[12] Karabalis DL, Huang F. 3-D foundation-soil-foundation interaction. In: Kassab AJ, Brebbia CA, editors. Boundary element technology IX. Southampton: Computational Mechanics Publications; 1994.
[13] Karabalis DL, Mohammadi M. 3-D dynamic foundation-soil-foundation interaction on layered soil. Soil Dyn Earthq Eng 1998;17:139–52.
[14] Lehmann L, Antes H. Dynamic structure–soil–structure interaction applying the Symmetric Galerkin Boundary Element Method (SGBEM). Mech Res Commun

2001;28:297–304.
[15] Qian J, Tham LG, Cheung YK. Dynamic cross-interaction between flexible surface footings by combined BEM & FEM. Earthq Eng Struct Dyn 1996;25:509–26.
[16] Bard P-Y, Chazelas JL, Guéguen PH, Kham MJ, Semblat F. Site-city interaction. In: Oliveira C, Roca A, Goula X, editors. Assessing and managing earthquake risk. Springer; 2006.
[17] Yahyai M, Mirtaheri M, Mahoutian M, Daryan AS. Soil structure interaction between two adjacent buildings under earthquake load. Am J Eng Appl Sci 2008;1:121–5.
[18] Padron LA, Aznarez JJ, Maeso O. Dynamic structure–soil–structure interaction between nearby piled buildings under seismic excitation by BEM–FEM model. Soil Dyn Earthq Eng 2009;29:1084–96.
[19] Bolisetti C, Whittaker AS. Seismic structure–soil–structure interaction in nuclear power plants structures. In: SMiRT. New Delhi; 2011.
[20] Mulliken JS, Karabalis DL. Discrete model for foundation-soil-foundation interaction. Soil dynamics and earthquake engineering VII. Southampton: CMP, Publications; 1995.
[21] Mulliken JS, Karabalis DL. Discrete model for dynamic through-the-soil coupling of 3D foundations and structures. Soil Dyn Earthq Eng 1998;27:678–710.
[22] Alexander NA, Ibraim E, Aldaikh H. A simple discrete model for interaction of adjacent buildings during earthquakes. Comput Struct 2013;124:1–10.
[23] Aldaikh H, Alexander NA, Ibraim E, Oddbjornsson O. Two dimensional numerical and experimental models for the study of structure-soil-structure interaction involving three buildings. Comput Struct 2015;150:79–91.
[24] Aldaikh H, Alexander NA, Ibraim E, Knappett J. Evaluation of rocking and coupling rotational stiffness coefficient of adjacent foundations. Int J Geomech, ASCE 2018;18(1):04017131.
[25] Vicencio F, Alexander NA. Dynamic interaction between adjacent buildings through nonlinear soil during earthquakes. Soil Dyn Earthq Eng 2018;108:130–41.
[26] Hans S, Boutin C, Ibraim E, Rousillon P. In situ experiments and seismic analysis of existing buildings. Part I: experimental investigations. Earthq Eng Struct Dyn 2005;34(12):1513–29.
[27] Li PZ, Hou XY, Liu YM, Lu XL. Shaking table model tests on dynamic structure- soil-structure interaction during various excitations. In: Proceedings of the 15th world conference on earthquake engineering. Lisbon (Portugal); 2012.
[28] Aldaikh H, Alexander N, Ibraim E, Knappett J. Shake table testing of the dynamic interaction between two and three adjacent buildings (SSSI). Soil Dyn Earthq Eng 2016;89:219–32.
[29] Knappett J, Massen P, Caucis K. Seismic structure-soil-structure interaction between pairs of adjacent building structures. Geotechnique 2015;65(5):429–41.
[30] Trombetta NW, Hutchinson TC, Mason HB, Zupan JD, Bray JD, Bolisetti C, et al. Centrifuge modeling of structure–soil–structure interaction: seismic performance of inelastic building models. In: Presented at the 15th world conference on earthquake engineering. Lisbon (Portugal); 2012.
[31] Trombetta NW, Mason HB, Chen Z, Hutchinson TC, Bray JD, Kutter BL. Nonlinear dynamic foundation and frame structure response observed in geotechnical centrifuge experiments. Soil Dyn Earthq Eng 2013;50:117–33.
[32] Mason HB, Trombett NW, Chen Z, Bray JD, Hutchinson TC, Kutter BL. Seismic soil–foundation–structure interaction observed in geotechnical centrifuge experiments. Soil Dyn Earthq Eng 2013;48:162–74.
[33] Kitada Y, Hirotani T, Iguch M. Models test on dynamic structure–structure interaction of nuclear power plant buildings. Nucl Eng Des 1999;192:205–16.
[34] Yano T, Naito Y, Iwamoto K, Kitada Y, Iguchi M. Model test on dynamic cross interaction of adjacent building in nuclear power plants – overall evaluation on field test, k06-2. In: Presented at the transactions of the 17th international conference on structural mechanics in reactor technology. Prague (Czech Republic); 2003.
[35] FEMA P695, Federal Emergency Management Agency. Quantification of building seismic performance factors, June 2009.
[36] SEAOC Bluebook. The recommended lateral force requirements of the structural. SEAOC; 1959.
[37] Chopra AK. Dynamics of structures: theory and applications to earthquake engineering. 2nd ed. Prentice-Hall; 2000.
[38] Newmark NM, Rosenblueth E. Fundamentals of earthquake engineering. Prentice-Hall; 1971.
[39] Gorbunov-Possadov MI, Serebrajanyi V. Design of structures upon elastic foundations. In: Presented at the 5th international conference soil mechanics foundation engineering. Paris; 1961.
[40] Clough RW, Penzien J. Dynamics of structures. 2nd ed. McGrawHill Int.; 1993.
[41] PEER Strong Motion Database < http://ngawest2.berkeley.edu/ > .
[42] Baker JW. Quantitative classification of near-fault ground motions using wavelet analysis. Bull Seismol Soc Am 2015;31:1486–501.